Global glacial isostatic adjustment and coastal tectonics

W. R. PELTIER

Department of Physics, University of Toronto, Toronto, Ont., Canada M5S 1A7
(e-mail: peltier@atmosp.physics.utoronto.ca)

Abstract: A global and gravitationally self-consistent model of the process of glacial isostatic adjustment (GIA) has been developed that extremely well reconciles the vast majority of available records of Holocene relative sea-level history, not only from sites that were ice covered at last glacial maximum (LGM) but also from sites that are well removed from such locations. There do exist, however, data that have been construed to constitute a significant challenge to this theory, namely, the long records of relative sea-level history derived on the basis of U/Th-dated coral sequences from the Huon Peninsula of Papua New Guinea and from Tahiti in the central equatorial Pacific Ocean. Following a review of the theoretical model and a discussion of the extent to which it is able to successfully reconcile a very wide range of Holocene shoreline observations, the discussion focuses upon the interpretation of these very important and interesting records, which are subject to different levels and types of tectonic contamination. These analyses suggest that existing estimates of the levels of Holocene tectonic contamination at both locations may require revision. In this context, it is suggested that the global model of the GIA process is sufficiently accurate that the magnitude and form of local tectonic effects during the Holocene period might be sensibly estimated by simply subtracting the GIA prediction for a given site from the observed variation of relative sea level.

The late Pleistocene cycle of glaciation and deglaciation, which has been the dominant contributor to climate system variability for the last 900 000 years of Earth history, is indelibly recorded in the geological record of relative sea-level (rsl) change. As each of these 100 000 year quasi-periodic cycles of ice-sheet advance and retreat involved a fall and subsequent rise of eustatic sea level of *c.* 120 m, it is hardly surprising that the record of these events should be of such high quality. The best proxy recordings of this glacial cycle, from a long timescale perspective, undoubtedly consist of those based upon oxygen isotopic measurements made on the tests of Foraminifera extracted from deep-sea sedimentary cores. Shackleton (1967) demonstrated that the records thereby derived on the basis of benthic species provided a high-quality proxy for the amount of land ice that existed on the continents at the time in the past represented by the depth in the core at which the isotopic measurement was made. It is, of course, on the basis of records of this kind that the important role played by orbital insolation variations in driving the ice-age cycle was first clearly established (Hays *et al.* 1976). Although the linkage between orbital insolation forcing and ice volume response is not nearly so direct as Milankovitch had envisioned (e.g. see Tarasov & Peltier (1997) for a recent discussion) it was nevertheless clear on the basis of such data that the small changes in the effective intensity of the Sun, caused by temporal variations of the geometric properties of the Earth's orbit, were able to induce significant cryospheric response.

Of primary interest in the present context will be the variations of rsl that are associated with the most recent deglaciation event, which began subsequent to last glacial maximum (LGM) 21 000 sidereal years ago. Even though this event had essentially ended by *c.* 4000 years ago, rsl continues to change owing to this cause (by rsl, in all that follows, I will imply sea level measured with respect to the surface of the solid Earth). This lingering memory of the deglaciation process is essentially a consequence of the fact that the Earth's shape is continuing to deform because of the shift in surface mass load that occurred during deglaciation as the vast Laurentide, Northwest European and southern hemisphere ice complexes disintegrated and the meltwater thereby produced was added to the ocean basins. This continuing deformation is a consequence of the very high value of the effective viscosity of the Earth's mantle, which governs the timescale of the return to gravitational equilibrium of the ice–solid earth–ocean system subsequent to deglaciation. Because this continuing relaxation of shape depends so strongly upon mantle viscosity, observations of the process may be employed to infer this Earth property and its variation with depth. That such inferences provide information of fundamental importance will be clear by virtue of the fact that knowledge of the steady-state creep resistance of the mantle is required in the construction of mantle convection models of the process of continental drift and sea-floor spreading.

In the discussion of these ideas to be presented in what follows, I will begin with a brief

PELTIER, W. R. 1998. Global glacial isostatic adjustment and coastal tectonics. *In*: STEWART, I. S. & VITA-FINZI, C. (eds) *Coastal Tectonics*. Geological Society, London, Special Publications, **146**, 1–29.

review of the theoretical structure of the global model of the glacial isostatic adjustment (GIA) process that has been under continuous refinement at Toronto for some time. The origins of this model lie in the analysis presented by Peltier (1974) of the viscoelastic response of spherically symmetrical models of the planet to variations of surface mass load. Using the impulse response Green function for the perturbation of the surface gravitational potential derived for such models by Peltier & Andrews (1976), Farrell & Clark (1976) discussed the primitive form of a 'Sea-level equation' that could be employed to predict the variations of rsl that should occur as a result of the combined influence of the deformation of the solid Earth caused by the changing surface load and the deformation of the geoid (the surface of constant gravitational potential that is coincident with mean sea level (msl) over the oceans). This equation was constructed by analogy with that introduced by Platzman (1971) to describe the influence of the elastic yielding of the sea floor onto the ocean tides. In the studies by Clark *et al.* (1978) and Peltier *et al.* (1978) this equation was more accurately expressed and solved for the realistic model of northern hemisphere deglaciation that had been produced by Peltier & Andrews (1976) and designated ICE-1. Further refinements to the theoretical structure that were thereafter introduced included the additional mathematical analysis required to calculate the rotational response to the glaciation–deglaciation process (Peltier 1982; Wu & Peltier 1984), analysis of the free air gravity anomalies associated with this dynamical forcing (Wu & Peltier 1983; Mitrovica & Peltier 1989; Peltier *et al.* 1992), more accurate spectral methods for the solution of the sea-level equation itself (Mitrovica & Peltier 1991) and development of a technique with which one might incorporate into the solution the full influence of time dependence of the coastline (Peltier 1994) and of the (rather less important) feedback of the changing rotational state of the planet onto sea-level history itself (Peltier 1998*a*, *b*). Various parts of this theoretical structure have been subsequently reproduced by others and the complete structure now serves as basis for the continuing international effort to fully understand the GIA process. These contributions from workers outside the Toronto group include those by Lambeck *et al.* (1990), who employed a much simplified version of the sea-level equation to investigate the postglacial rebound of Fennoscandia; Lambeck *et al.* (e.g. 1996), who performed a detailed series of analyses of postglacial rsl histories of the British Isles; Han & Wahr (1995), who have rederived the viscoelastic normal mode formalism of Peltier (1976, 1985); and Fang & Hager (1995), who have also invested effort to understand the rudiments of the normal mode theory. The implications of this work to our understanding of mantle rheology have also been thoughtfully addressed in the recent literature by Karato & Wu (1993).

In the following section of this paper I briefly review the structure of this formal theory of the GIA process. I will then focus upon the problem of tuning the viscosity profile of the model, and will examine the extent to which the theory is able to accurately reconcile a globally distributed set of rsl histories obtained on the basis of ^{14}C dating of various rsl indicators. Given the rather good fit to such data that the model delivers, further analyses are devoted to the investigation of observations that have been suggested to disagree profoundly with the theoretical predictions. Arguments are presented to the effect that these concerns are not particularly well founded, and conclusions are offered.

The global theory of GIA and rsl change

The record of sea-level history that is contained in the geological record is a recording of the level of the sea relative to the deforming surface of the solid Earth. It is this fact which makes the interpretation of the record as challenging as it so clearly is. If we define this rsl history to be $S(\theta, \lambda, t)$, with θ and λ latitude and longitude, respectively, and t time, then we might usefully express rsl history in the following schematic fashion:

$$S(\theta, \lambda, t) = C(\theta, \lambda, t)[G(\theta, \lambda, t) - R(\theta, \lambda, t)] \quad (1)$$

in which $C(\theta, \lambda, t)$ is the so-called 'ocean function', which equals zero over land or land-locked water and unity over the surface of the global ocean. In equation (1), $G(\theta, \lambda, t)$ is the geoid of classical geodesy which is defined by the surface of constant gravitational potential that is coincident with msl over the oceans and $R(\theta, \lambda, t)$ is the local radius of the solid Earth. To predict the function $S(\theta, \lambda, t)$ we are therefore obliged to develop a theory on the basis of which we may compute the triplet of functions (C, G, R). The key ingredient of such a theory, as previously mentioned, was provided by Peltier (1974) who developed a mathematical structure with which one could calculate both G and R assuming C to be fixed to the present-day ocean function.

That analysis, which was based upon the application of first-order perturbation theory, led to

the re-expression of equation (1) in the form:

$$S(\theta,\lambda,t) = C(\theta,\lambda,t) \times \left\{ \int_{-\infty}^{t} dt' \int_{\Omega}\int d\Omega\, L(\theta',\lambda',t') \times \left\{ \frac{\phi^{L}(\gamma,t-t')}{g} - \Gamma^{L}(\gamma,t-t') \right\} + \frac{\Delta\Phi(t)}{g} \right\} \quad (2)$$

in which Ω is the surface of the Earth, L is the history of variations of surface mass load (mass per unit area) that occur as a result of the glaciation–deglaciation process, ϕ^{L} and Γ^{L} are respectively viscoelastic surface load Green functions for the gravitational potential perturbation and radial displacement, and the function $\Delta\Phi(t)$ is constructed so as to ensure that the variation of surface mass load is mass conserving in the sense that only the mass of water produced by melting (or accreting) continental ice appears in (or disappears from) the oceans. The argument γ in these Green functions is simply the angular separation between source point (θ',λ') and field point (θ,λ), a spatial dependence which results from the assumption that the Earth model of interest is spherically symmetrical in its physical properties. From a mathematical perspective the right-hand side of equation (2) is a (triple) convolution integral. The theory required to construct ϕ^{L} and Γ^{L} was presented by Peltier (1974) and Peltier & Andrews (1976), and requires knowledge only of the radial viscoelastic structure of the planet. From a technical perspective the challenge posed by equation (2) arises because of the composite property of the surface load L. This may be made explicit by expanding it in the form

$$L(\theta,\lambda,t) = \rho_{I} I(\theta,\lambda,t) + \rho_{w} S(\theta,\lambda,t) \quad (3)$$

in which ρ_{I} and ρ_{w} are the densities of ice and water, respectively, and I and S are respectively ice and water 'thickness'. We consider L to be positive when the net mass per unit area is increasing and negative where it is decreasing.

Clearly, when equation (3) is inserted in equation (2) the resulting equation will be seen to constitute an integral equation for the rsl history $S(\theta,\lambda,t)$, as S now appears not only on the left-hand side but also under the triple convolution integral on the right-hand side. Given an assumed history of ice-sheet thickness variations $I(\theta,\lambda,t)$ and a radial viscoelastic structure for an assumed spherically symmetrical model of the planetary interior, we could proceed to solve this integral equation to predict $S(\theta,\lambda,t)$ and to compare these predictions with geologically inferred rsl histories. In this process we would construct the function $\Delta\Phi(t)$ such as to ensure conservation of mass by insisting that

$$\int_{c} \rho_{w} S(t)\, d\Omega = \int_{c} \rho_{w} \left\{ \int_{-\infty}^{t} dt' \int_{\Omega}\int d\Omega'\, L(\theta'\phi',t') \times [G(t-t') - R(t-t')] \right\} d\Omega + \frac{\Delta\Phi(t)}{g} \cdot \rho_{w} A = -M_{I}(t) \quad (4)$$

in which the integral on the left-hand side is the mass that has been added to the oceans by time t, which must equal the mass of water produced by melting ice, here defined as $M_{I}(t)$. The negative sign affixed to this function on the right-hand side of equation (4) is employed to indicate explicitly that $M_{I}(t)$ itself is negative when this component of the surface mass load is being removed from the surface. By defining

$$\frac{\Phi(t)}{g} = -\frac{M_{I}(t)}{\rho_{w} A(t)} - \frac{1}{A(t)} \times \left\langle \int_{-\infty}^{t} dt' \int_{\Omega}\int d\Omega'\, L(\theta',\phi',t') \times [G(t-t') - R(t-t')] \right\rangle_{o} \quad (5)$$

in which $A(t)$ is the surface area of the oceans at time t and $\langle\rangle_{o}$ indicates integration over the oceans, we will then ensure that solutions to equation (2) conserve mass. Because of the form of the $\Delta\Phi(t)/g$ correction to equation (2), one should not expect that the amount of sea-level rise that occurs far from the ice sheets will be well approximated by the first term on the right-hand side of equation (5).

Although it is precisely the form of the sea-level equation (2) that I have employed as basis for most of my work on the GIA process, there are in fact two potentially relevant physical effects that are not included in this version of the theory. These are, respectively, the influence of the time dependence of the ocean function $C(\theta,\lambda,t)$ and the feedback onto sea level of the changing rotational state of the planet. I will return to a discussion of the important former effect below. The latter effect turns out to be small but it is difficult to be certain that this is so without actually doing the calculation. To accomplish this we proceed iteratively by first solving equation (2) to determine the global rsl history S by assuming C to be constant and

including a model of the history of ice-sheet loading and unloading before LGM (this may be constructed by employing the SPECMAP $\delta^{18}O$ record of Imbrie *et al.* (1984)). Given the complete history of surface mass loading L, we then solve the Euler equation

$$\frac{\mathrm{d}}{\mathrm{d}t}(J_{ij}\omega_j) + \varepsilon_{ijk}\omega_j J_{kl}\omega_l = 0 \tag{6}$$

in which J_{ij} is the moment of inertia tensor of the planet, ω_j are the components of its angular velocity vector and ε_{ijk} is the Levi–Cevita alternating tensor. Assuming a biaxial model for the undeformed shape of the planet (see Peltier & Jiang (1996*a*) and Peltier (1997) for the complete but unnecessary triaxial theory), highly accurate solutions to equation (6) may be constructed by employing the standard perturbation expansion:

$$\begin{aligned} \omega_i &= \Omega(\delta_{ij} + m_i) \\ J_{ij} &= I_{ij}, i \neq j \\ J_{11} &= A + I_{11} \\ J_{22} &= A + I_{22} \\ J_{33} &= C + I_{33} \end{aligned} \tag{7}$$

in which (A, A, C) are the principle moments of inertia, Ω is the angular velocity of the unperturbed Earth, and I_{ij} and m_i are assumed small fluctuations away from the unperturbed basic state. On substitution of equation (7) into equation (6) and dropping all terms of higher order than first in the fluctuations we obtain the following decoupled system of equations for polar motion and rotation, respectively:

$$\frac{i}{\sigma_r}\dot{\boldsymbol{m}} + \boldsymbol{m} = \Psi \tag{8a}$$

$$\dot{m}_3 = \Psi_3 \tag{8b}$$

in which the so-called excitation functions are Ψ and Ψ_3, $\sigma_r = (C - A)\Omega/A$ is the Chandler wobble frequency of the rigid Earth, $\boldsymbol{m} = m_1 + im_2$, $\Psi = \Psi_1 + i\Psi_2$, $i = \sqrt{-1}$ and the Ψ_i are, with the dot indicating time differentiation, respectively,

$$\Psi_1 = \frac{I_{13}}{(C - A)} + \frac{\dot{I}_{23}}{\Omega(C - A)} \tag{9a}$$

$$\Psi_2 = \frac{I_{23}}{(C - A)} - \frac{\dot{I}_{13}}{\Omega(C - A)} \tag{9b}$$

$$\Psi_3 = -\frac{I_{33}}{C} \tag{9c}$$

As discussed in detail by Peltier (1982) and Wu & Peltier (1984), equations (8) may be solved most efficiently by using Laplace transform techniques to determine the $\omega_i(t)$ once $L(\theta, \lambda, t)$ has been fully determined by solving the sea-level equation (2).

Given the solution to equation (8) we may simply incorporate the influence of the changing rotation into equation (2) by extending it as:

$$\begin{aligned} S(\theta, \lambda, t) = C(\theta, \lambda, t)\Bigg\{ & \int_{-\infty}^{t} \mathrm{d}t' \int_{\Omega}\int \mathrm{d}\Omega' \\ & \times \Big[L(\theta', \lambda', t') G_{\phi}^{\mathrm{L}}(\gamma, t - t') \\ & + \Psi^{\mathrm{R}}(\theta', \lambda', t') G_{\phi}^{\mathrm{T}}(\gamma, t - t') \Big] \\ & + \frac{\Delta\Phi(t)}{g} \Bigg\} \end{aligned} \tag{10}$$

in which the Green function $G_{\phi}^{\mathrm{L}} = [\phi(\gamma, t - t')/g - \Gamma(\gamma, t - t')]$ is the same kernel as in equation (2), $\Psi^{\mathrm{R}}(\theta', \lambda', t')$ is the variation of the centrifugal potential because of the changing rotational state which, following Dahlen (1976), may be written (to first order in perturbation theory, to be consistent with the approximation employed to solve equation (6)), as

$$\Psi^{\mathrm{R}} = \Psi_{\mathrm{oo}} Y_{\mathrm{oo}}(\theta, \lambda) + \sum_{m=-1}^{+1} \Psi_{2m} Y_{2m}(\theta, \lambda) \tag{11}$$

where

$$\begin{aligned} \Psi_{\mathrm{oo}} &= \tfrac{2}{3}\omega_3(t)\Omega a^2 \\ \Psi_{20} &= -\tfrac{1}{3}\omega_3(t)\Omega a^2\sqrt{4/5} \\ \Psi_{2-1} &= (\omega_1 - i\omega_2)(\Omega a^2/2)\sqrt{2/15} \\ \Psi_{2+1} &= (\omega_1 + i\omega_2)(\Omega a^2/2)\sqrt{2/15} \end{aligned}$$

and the tidal-loading Green function G_{ϕ}^{T} is expressed in terms of tidal Love numbers h_l^{T} and k_l^{T} as

$$G_{\phi}^{\mathrm{T}}(\gamma, t) = \frac{1}{g}\sum_{l=o}^{\infty} [1 + k_l^{\mathrm{T}}(t) - h_l^{\mathrm{T}}(t)] P_l(\cos\gamma) \tag{12}$$

just as the surface-loading Green function G_{ϕ}^{L} is expressed in terms of surface load Love numbers h_l^{L} and k_l^{L} as

$$G_{\phi}^{\mathrm{L}}(\gamma, t) = \frac{a}{me}\sum_{l=o}^{\infty} [1 + k_l^{\mathrm{L}}(t) - h_l^{\mathrm{L}}(t)] P_l(\cos\gamma) \tag{13}$$

Both sets of viscoelastic Love numbers are calculated using the theoretical ideas and methods developed by Peltier (1974, 1976, 1985). There will be no purpose served by reviewing these technical details here.

A further aspect of theory that will be of particular interest, however, is that required to incorporate the full impact of the changing coastline that occurs as land becomes inundated by the sea as sea levels rise because of ice-sheet melting and as land that was once ice covered rises out of the sea as a result of the process of postglacial crustal 'rebound'. To understand how these additional influences may be incorporated into the theory it is helpful to begin by noting that both forms of the 'sea-level equation', namely, those represented by equations (2) and (10), are constructs of first-order perturbation theory that deliver solutions for the history of rsl change with respect to an unspecified and thus arbitrary datum. It is precisely this arbitrariness that may be exploited so as to incorporate the full influence of ocean function time dependence. We simply fix this datum by determining a time-independent field $T'(\theta, \lambda)$ such that

$$S(\theta, \lambda, t_p) + T'(\theta, \lambda) = T_p(\theta, \lambda)$$

in which S is a solution to either equation (2) or (10), t_p is the present time and $T_p(\theta, \lambda)$ is the present-day topography of the planet with respect to sea level determined, say, by the ETOPO5 model (or some other higher-resolution model if one is available). If we then construct a time-dependent topography for the planet by computing

$$T(\theta, \lambda, t) = S(\theta, \lambda, t) + [T_p(\theta, \lambda) - S(\theta, \lambda, t_p)]$$

and correct this by adding to $T(\theta, \lambda, t)$ the thickness of ice $I(\theta, \lambda, t)$ to obtain

$$\begin{aligned} PT(\theta, \lambda, t) &= T(\theta, \lambda, t) + I(\theta, \lambda, t) \\ &= S(\theta, \lambda, t) + T'(\theta, \lambda) + I(\theta, \lambda, t) \end{aligned} \tag{14}$$

it will be clear that where $T + I$ is positive there is (perhaps ice-covered) land that stands above sea level and that where $T + I$ is negative there is ocean. We may then define a 'first estimate' of the time-dependent ocean function as the function $C^1(\theta, \lambda, t)$ that is unity wherever $T + I$ is negative. Given this first estimate we then return to equation (2) or (10) and solve it again incorporating this form of the time dependence of $C(\theta, \lambda, t) = C^1(\theta, \lambda, t)$. Given the new solution $S(\theta, \lambda, t)$, we then determine a new $T'(\theta, \lambda)$ and thus a new $C = C^2(\theta, \lambda, t)$ using equation (14). We continue this iterative process until the solution for $C(\theta, \lambda, t)$ converges, which typically occurs in just a few iterations.

Very recently, a further refinement of this theory has been developed which has both increased the accuracy of the computation of palaeotopography as defined in equation (14) and improved the understanding of mass balance when this is examined from the perspective of the eustatic sea-level rise expected on the basis of the total ice melt and the net sea-level rise that is predicted by solving equation (2) or (10). This involves a subtle aspect of the theory that has not been explored until recently (Peltier 1998*c*) which is as follows. We consider the evolution of rsl $S_{IS}(\theta, \lambda, t)$ at a point on the landscape that is ice covered at LGM but which later comes to be inundated by the sea. Here I employ the subscript IS to denote inland sea. At such points the time series for S_{IS} that is delivered by solving equation (2) or (10) has the following mathematical form:

$$\begin{aligned} S_{IS}(\theta, \lambda, t \geq t_D) &= \Delta S_{IS}(\theta, \lambda) H(t - t_D) \\ &\quad + S'_{IS}(\theta, \lambda, t \geq t_D) \end{aligned} \tag{15}$$

in which $t_D(\theta, \lambda)$ is the time of 'deglaciation' when the sea first occupies the region at latitude θ and longitude λ, $\Delta S_{IS} < 0$ is a spontaneous fall of sea level that is delivered by the solution of equation (2) or (10) at the instant t_D, $H(t - t_D)$ is the Heaviside step function ($+1$ for $t \geq t_D$ and zero for $t < t_D$) and $S'_{IS}(\theta, \lambda, t \geq t_D)$ is a function that vanishes at $t = t_D$ and thereafter decreases with time so as to represent the fall of rsl that occurs in the inland sea as a consequence of postglacial rebound of the crust. Solutions to equation (2) or (10) deliver an abrupt fall of sea level at $t = t_D$ because at that instant there is a marked difference in the gravitational potential between such locations and that which defines the surface of the exterior ocean with this potential being higher than the surface ocean because of the influence of glacial rebound. Solutions to equation (2) or (10) therefore deliver a sharp drop of sea level at the instant of deglaciation $t = t_D$ even though the region is being inundated. This is a source of mass to the exterior ocean and constitutes an additional removal of load from the deglaciating region. As this removal of load can only represent, in fact, an additional removal of ice, it is clear that ΔS_{IS} is actually to be associated with an 'implicit' component of the ice unloading history. I call this 'implicit ice' and its contribution to the loading history, expressed in

terms of an equivalent ice thickness, may be computed from the expression

$$L(\theta, \lambda, t) = \rho_I I_{EX}(\theta, \lambda, t) + \rho_w \Delta S_{IS} H(t - t_D)$$
$$= \rho_I \left[I_{EX}(\theta, \lambda, t) + \frac{\rho_w}{\rho_I} \Delta S_{IS} H(t - t_D) \right]$$
$$= \rho_I [I_{EX}(\theta, \lambda, t) + I'_{IM}(\theta, \lambda, t)] \quad (16a)$$

in which $I_{EX}(\theta, \lambda, t)$ is the ice thickness history determined by tuning the model (see below) to fit rsl observations from the ice-covered region, and $I'_{IM}(\theta, \lambda, t)$ is the implicit ice that was also removed to deliver the mass to the exterior ocean that is obtained from the solution of equation (2) or (10). In this solution the ice load I_{IM} 'masquerades' as a fall of sea level.

A second contribution to the implicit component of the ice load is connected to the field $S(\theta, \lambda, t)$ in equation (15). It will be clear that, for rsl to be able to fall in regions that were ice covered at LGM but which are inundated by the sea at $t = t_D$, there must be water in the ice-covered region subsequent to t_D! Now, in the solution of equation (2) or (10), the unloading of these regions is fully accounted for, partly by I_{EX} and partly by I^1_{IM}. What is not accounted for, in this equation that derives from the application of first-order perturbation theory, is the net mass of water that fills the depression of the surface that exists at $t = t_D$. This water must, of course, also be delivered by the ice that disappeared from the surface as inundation occurred. This additional contribution to the net implicit ice applies no load to the surface at $t = t_D$, only subsequently as rebound occurs, but it does contribute to the thickness of ice that must have existed on the surface at LGM and thus to the palaeotopography defined in equation (14). It may also be computed very accurately as follows. We simply compute the present altitude of the marine limit with respect to msl as a function of geographical position, say $ML(\theta, \lambda, t_p)$, and to this we add the present-day bathymetry, say $D(\theta, \lambda, t_p)$, to obtain, in ice thickness equivalent form, this second contribution to implicit ice as

$$I^2_{IM} = \frac{\rho_w}{\rho_I} [ML(\theta, \lambda, t_p) + D(\theta, \lambda, t_p)] \quad (16b)$$

In computing the full palaeotopography in equation (14) we must therefore also include this second contribution from implicit ice to obtain

$$PT(\theta, \lambda, t) = T(\theta, \lambda, t) + I_{EX}(\theta, \lambda, t) + I^1_{IM}(\theta, \lambda, t) + I^2_{IM}(\theta, \lambda, t)$$

Examples of the results obtained from this refinement of the palaeotopography calculation will be provided in what follows.

Before employing this theory to illustrate in detail the extent to which postglacial rsl histories may be explained in terms of it, it will be useful to first illustrate the general forms that such solutions possess. To this end I will immediately consider the nature of the solution obtained when the radial variation of mantle viscosity is fixed to that of model VM2 shown in Fig. 1. The origins of this model will be described in the next section. With the radial elastic structure of the model also fixed to that of the Preliminary Reference Earth Model (PREM; Dziewonski &

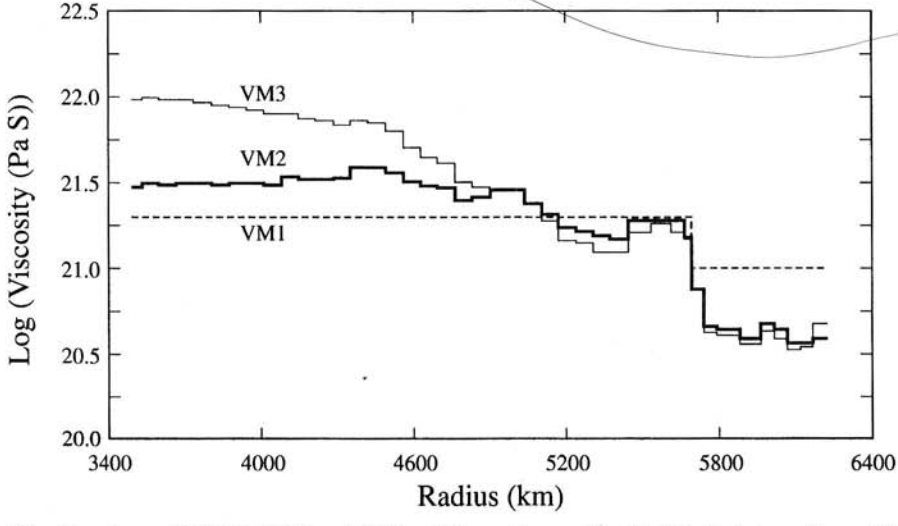

Fig. 1. The viscosity models VM1, VM2 and VM3, which are discussed in detail in the later sections of the text.

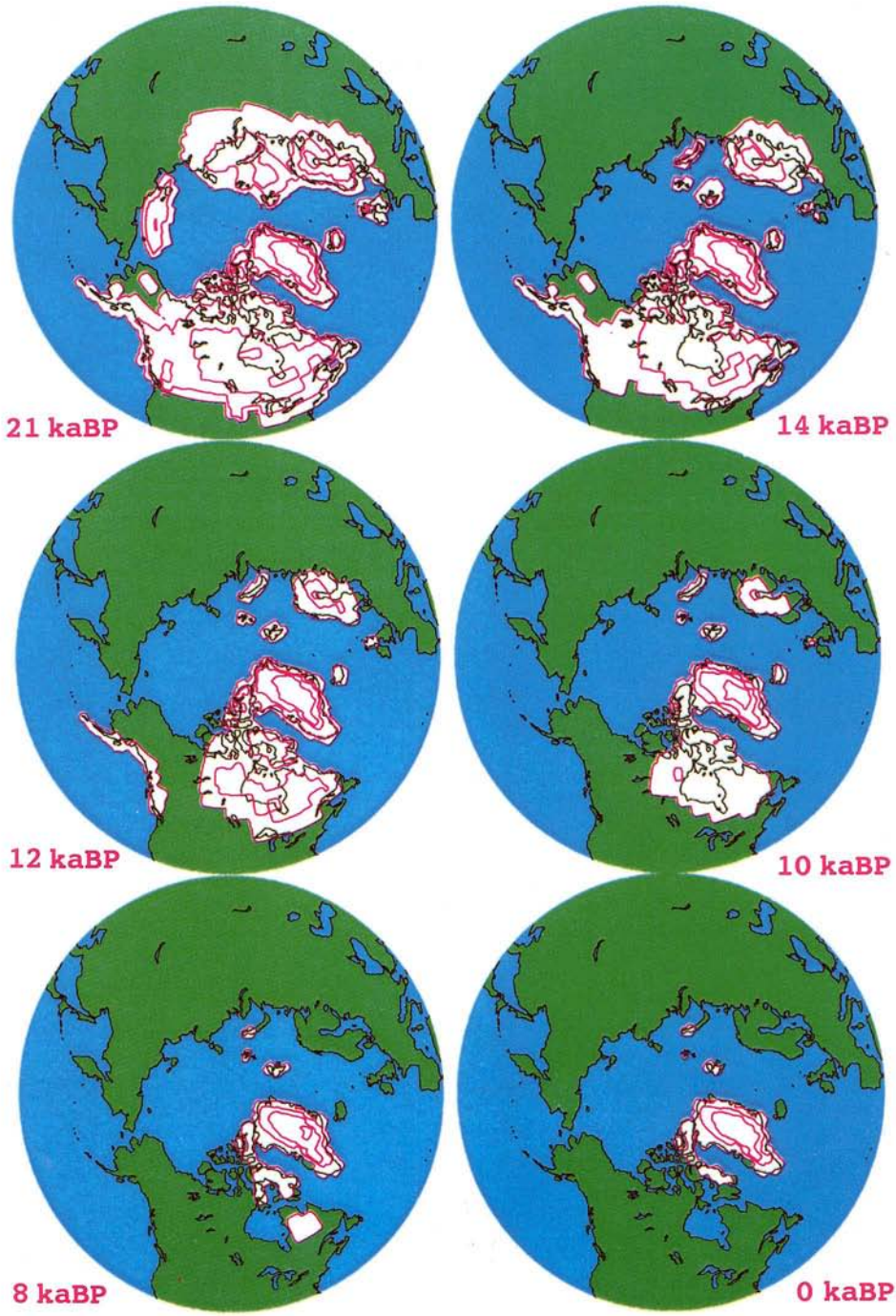

Fig. 2. Time slices through the ice-thickness maps that constitute the ICE-4G model of deglaciation (note that these are slightly modified from the fields derived by Peltier (1994, 1996), primarily by an increase of the ice thickness over the Laurentide complex that was centred on Hudson Bay).

Anderson 1981), solutions will be discussed for the ICE-4G deglaciation model of Peltier (1994), examples of the northern hemisphere isopacks for which are shown in Fig. 2. Notable in this figure are the extensive North American and Northwest European ice complexes that existed at LGM in which the thicknesses of the continental ice sheets, were typically of order 4 km. In the southern hemisphere component of ICE-4G there was also significantly more ice at LGM than at present over West Antarctica and also significant ice cover over Western Patagonia.

In Fig. 3 I show the present-day predicted rate of rsl rise for these choices of the input fields and for both the version of the sea-level equation that excludes the influence of rotational feedback (equation (2)) and that which includes this effect (equation (10)). The top and middle plates of Fig. 3 show these respective solutions, whereas the bottom plate displays the difference between them. Evident upon inspection of these illustrative results is that the influence of rotational feedback upon this characterization of the sea-level response to deglaciation is extremely weak and is strongly dominated by the degree two and order one pattern that is forced entirely (see equation (11)) by the polar motion component of the rotational response to deglaciation. That the influence of rotational feedback is weak not only from the perspective of the present-day rate of rsl rise driven by the GIA process but also from the perspective of the complete history of rsl change is demonstrated in Fig. 4, where I have compared predicted and observed rsl histories at six different locations. The first two, from Barbados and the Huon Peninsula, are U/Th-dated coral records that will figure prominently in what is to follow. The remaining four are from sites that are as close as possible to the extrema of the degree two and order one pattern that characterizes the contribution to the rsl record by rotational feedback. Even at these locations, where the influence of the feedback is most intense, it is clearly extremely weak and negligible for most purposes. This contradicts the claim to the contrary made recently by Bills & James (1996).

One final aspect of the general form of the solution upon which I will comment here concerns the time-dependent topography of the planet with respect to sea level that develops as a result of the deglaciation process. Figure 5 illustrates the northern hemisphere component of this field determined for the ICE-4G (VM2) model by executing the steps described in equations (14)–(16). Evident by inspection of this figure will be the vast land bridges that existed at LGM in both the present-day Bering Strait, which was then entirely dry land (the continent of 'Beringia'), and the present-day English Channel. At that time, most of the present-day Indonesian Archipelago was dry land, and a vast land bridge also connected Australia to Papua New Guinea. These aspects of the global 'topographically self-consistent' solution to the sea-level equation were first described by Peltier (1994). Figure 6 illustrates the time dependence of the coastline in several of these locations in terms of what I have previously called 'inundation maps', on the basis of which one may infer at a glance the time at which a particular land bridge first became impassible. Also of note in the second plate of Fig. 6, which simply portrays the regions of the Aegean Archipelago and Mediterranean Sea that are predicted to have been dry land at LGM but which are now beneath the sea, is that there are many candidates for Atlantis!

Tuning the model parameters

Although some evidence has already been presented to the effect that the ICE-4G (VM2) model successfully fits a considerable range of rsl observations, it will prove useful, before providing a more systematic demonstration of this fact, to discuss the procedure that has been followed to arrive at the two required input components of this model. These components consist respectively of the radial viscosity profile (VM2) and the deglaciation history (ICE-4G). As the model of deglaciation history has been discussed at length by Peltier (1994, 1996), I will focus herein on the viscosity structure.

Focusing then upon the radial profile of mantle viscosity, the profile VM2, or rather the family of VM2-like profiles, has been inferred (Peltier 1996, 1998*b*; Peltier & Jiang 1996*b*, 1997) through application of a formal Bayesian inversion procedure based upon the use of the simple VM1 profile shown in Fig. 1 as starting model. As a first estimate of the viscosity profile, VM1 has several properties which strongly suggest it to be highly appropriate. Of these, the most important will be clear on the basis of inspection of Fig. 7, which shows a sequence of predictions of the non-tidal acceleration of planetary rotation (represented by $\dot{J}_2$, which is the time rate of change of the degree two axial component of the gravitational potential field of the planet) and the speed of polar wander as a function of the viscosity of the lower mantle with the upper mantle and transition-zone viscosity fixed to 10^{21} Pa s. In each of these calculations the lithospheric thickness has been held fixed to

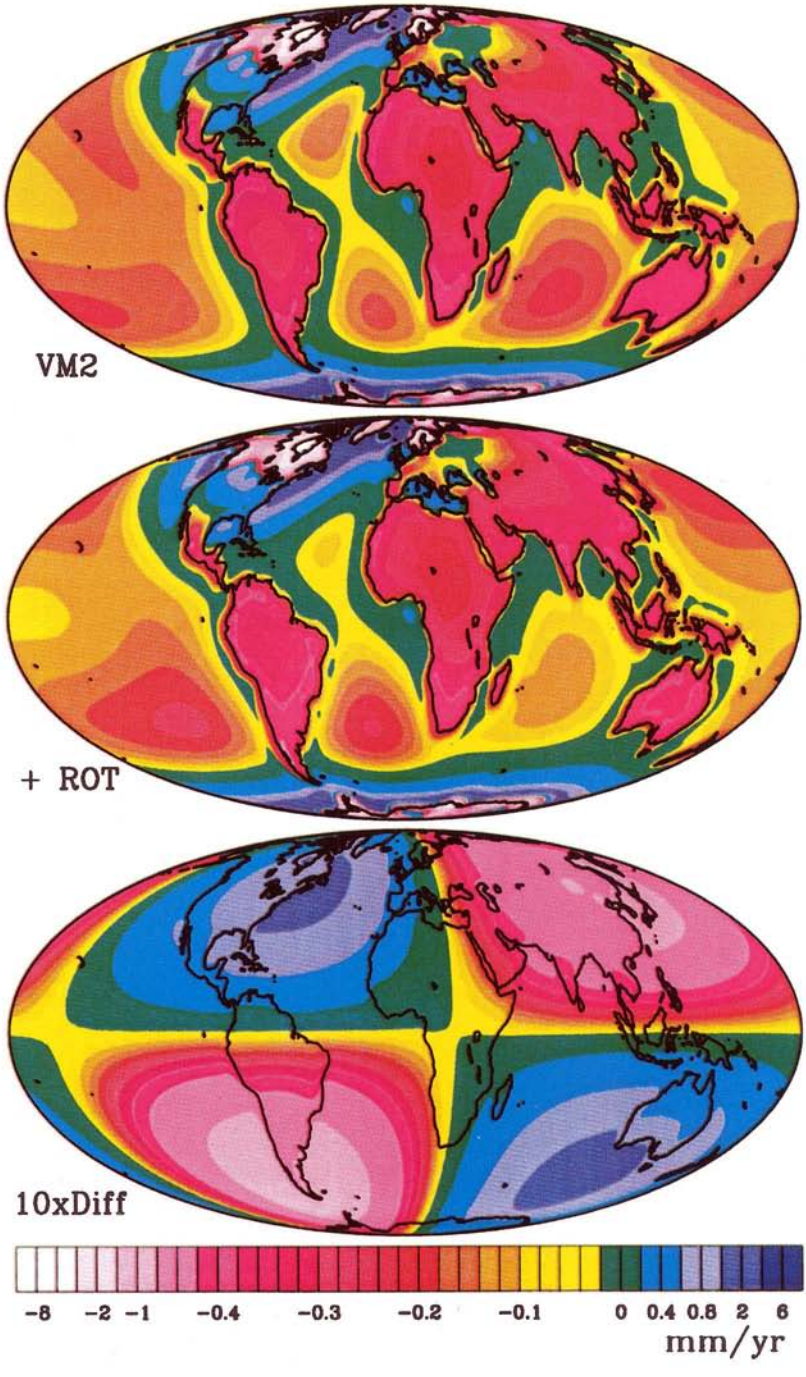

Fig. 3. Predictions of the present-day rate of rsl rise using the VM2 viscosity model and the ICE-4G deglaciation history. Results are shown for analyses performed that both exclude (top plate) and include (central plate) the influence of rotational feedback and (bottom plate) the difference between these predictions, which isolates the influence of the changing rotation alone.

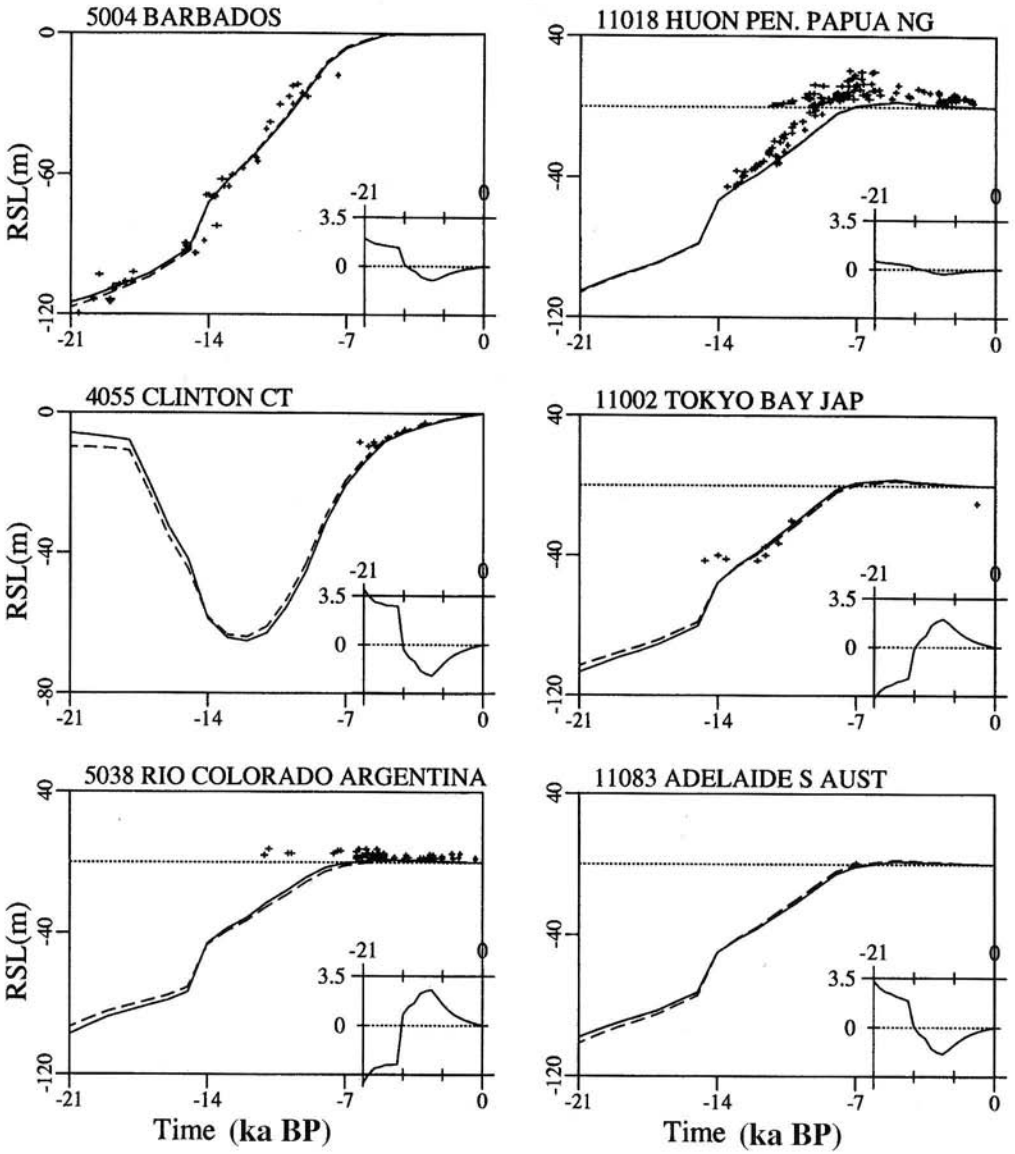

Fig. 4. Relative sea-level histories at six significant locations illustrating the negligibly weak impact of rotational feedback upon the Holocene record. The Barbados and Huon Peninsula sites are the two primary locations from which coral-based records are available. For the latter site only the raw data are shown, uncorrected for any influence of tectonic uplift. The final four sites are located as close as possible to the centres of the degree two and order one structure that characterizes the contribution of rotational feedback on rsl history. It is at these locations that the influence of this feedback is maximum. The continuous curve in each frame represents the rsl history that includes rotational feedback whereas the dashed curve is that obtained excluding this effect. The inset in each plate represents the difference between these two histories on a scale that ranges between −3.5 m and +3.5 m. Both sets of calculations were performed with the ICE-4G (VM2) model.

120.6 km. In Fig. 7a and b the range of the observed values of these properties of Earth's present-day rotational state (see Peltier & Jiang (1996*b*) and Peltier (1997), for a full discussion) is shown as the hatched region. Inspection of these results will demonstrate that both of these rotational observables are fitted by precisely the same viscosity model, namely that labelled VM1 in Fig. 1, as the value of lower-mantle viscosity preferred by both observations is seen to be

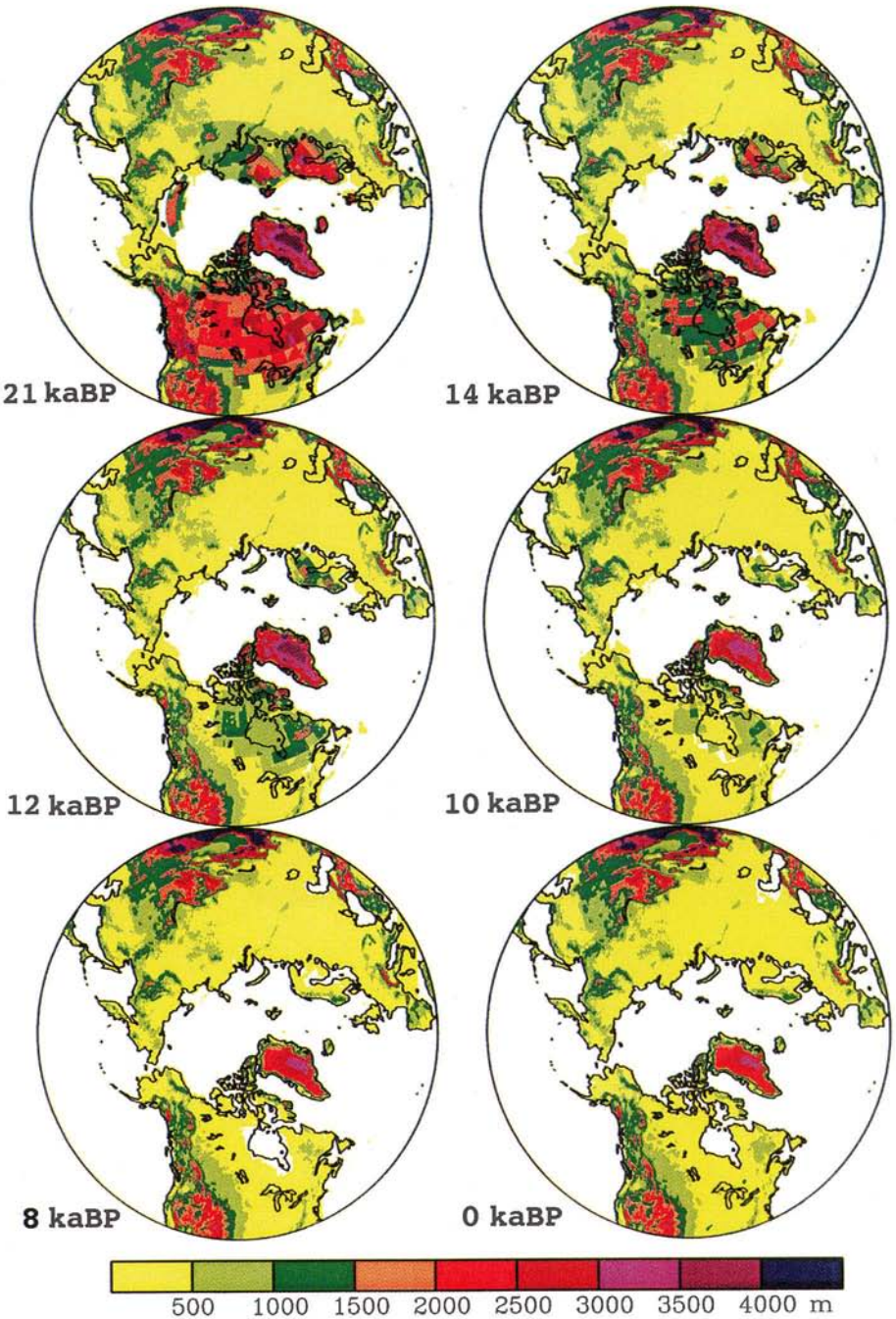

Fig. 5. Time-dependent topography of the northern hemisphere of the planet from LGM to present according to the ICE-4G (VM2) model of the GIA process. These results include the contributions from both explicit and implicit ice.

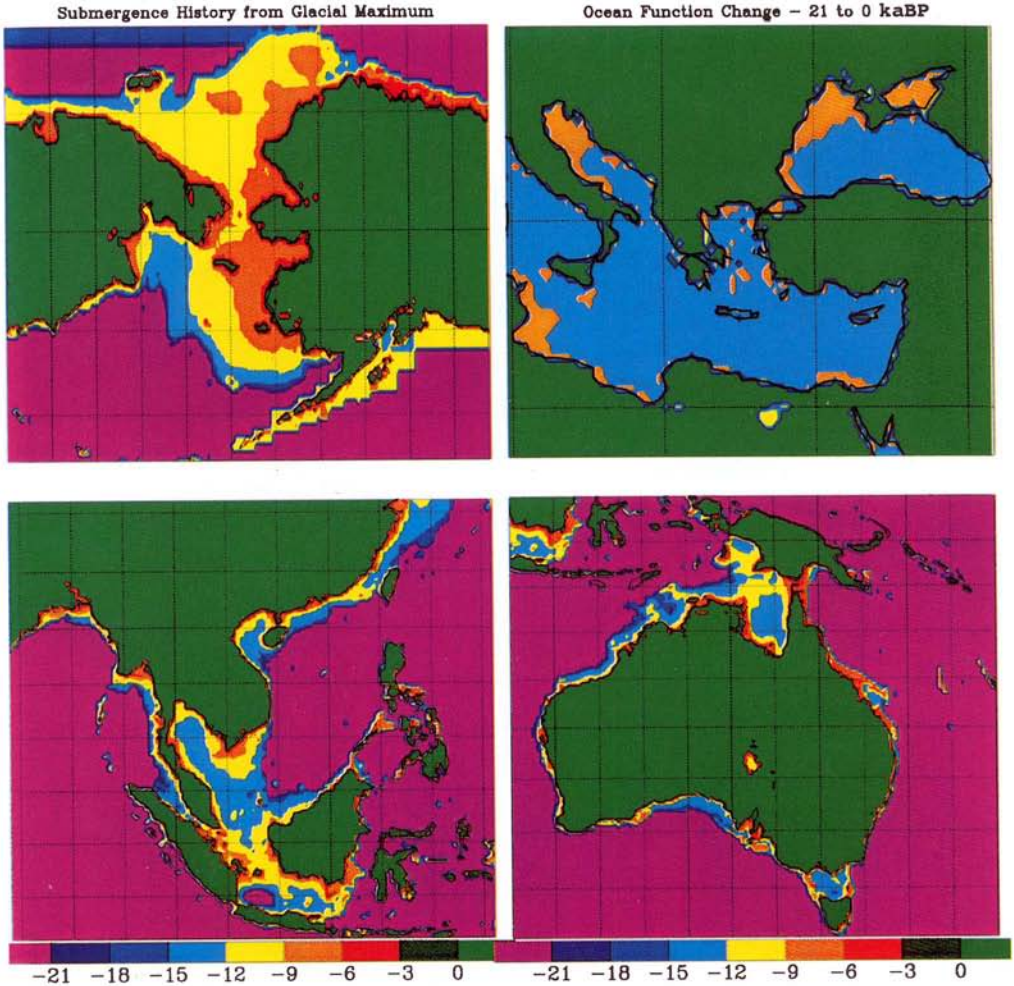

Fig. 6. Inundation maps for the Bering Strait, Australia–Papua New Guinea and the Indonesian Archipelago. Also shown is a map centred on the Greek archipelago showing the regions that would have been dry land at LGM (shown as beige) but which are today sea covered.

2×10^{21} Pa s. Because these rotational observables depend upon entirely independent components of the moment of inertia tensor (see equations (9)) it is highly unlikely, in my view, that they could be reconciled by precisely the same model of the radial viscoelastic structure if both observables were not primarily controlled by the GIA process. Furthermore, these rotational data are sensitive essentially to the average value of the viscosity from the base of the lithosphere to the core–mantle boundary (cmb). This may be seen by computing the Fréchet kernel $\mathrm{FK}^{\mathrm{R}}(r)$ for either of the rotational data, as this appears in the expression for the perturbation of an arbitrary measure of the response δR that is induced by a perturbation in the viscosity model $\delta \log_{10} \nu(r)$ as

$$\delta R = \int_b^a r^2 \mathrm{FK}^{\mathrm{R}}(r) \delta \log_{10} \nu(r)\, \mathrm{d}r \qquad (17)$$

in which b and a are the radii of the cmb and the Earth, respectively. The Fréchet kernels for each of the rotational data, computed at the model VM1, are shown in Fig. 8c. Because these functional derivatives for both $\dot{J}_2$ (J2) and polar wander speed (PW) are very slowly varying functions of radius r it is clear from equation (17) that these data determine essentially the average value of $\nu(r)$ through the

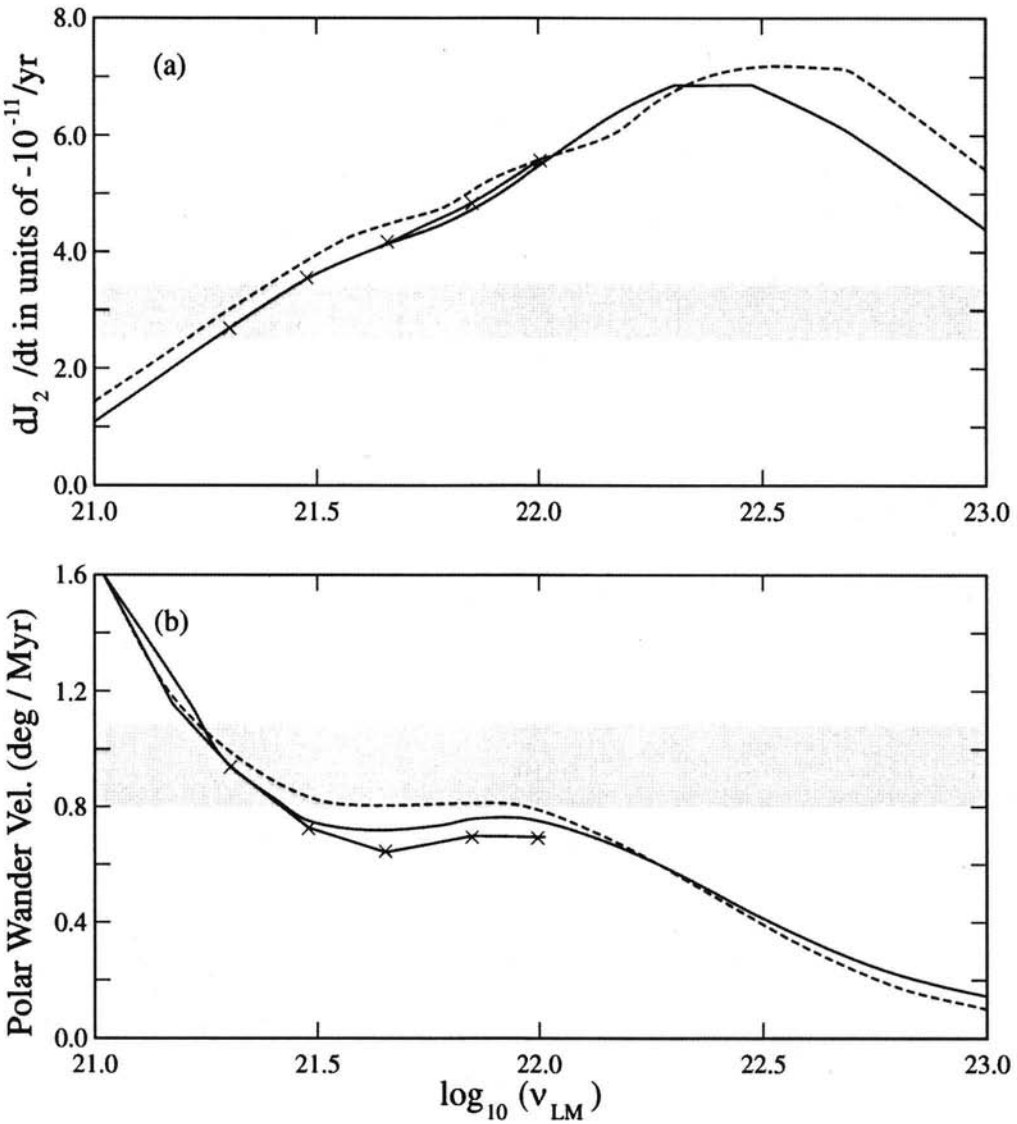

Fig. 7. (**a**) $\dot{J}_2$ as a function of lower-mantle viscosity ν_{LM} when the upper-mantle and transition zone viscosity is fixed to the value $\nu_{UM} = 1.0 \times 10^{21}$ Pa s and the lithospheric thickness is $L = 120.6$ km. Results are shown for both of the models of glaciation history for which inertia perturbations are shown in Fig. 3. (**b**) Polar wander speed as a function of lower-mantle viscosity ν_{LM}, with other parameters as in (**a**).

mantle. Because VM1 fits both observations it seems clear that this model has the correct value of this Earth property.

However, it is also clear that this model does not provide an acceptable fit to all data related to the GIA process. An extremely important example of a dataset that is not fitted by the VM1 model consists of the relaxation spectrum for Fennoscandian rebound originally inferred by McConnell (1968). His analysis of the strandline data for the post-glacial recovery of this region led him to infer the variation of relaxation time (shown as its inverse) as a function of spherical harmonic degree l shown in Fig. 9, in which the star symbol plotted adjacent to the low-degree asymptote at a relaxation time near 4600 years represents the relaxation time inferred by a Monte Carlo derived exponential fit to

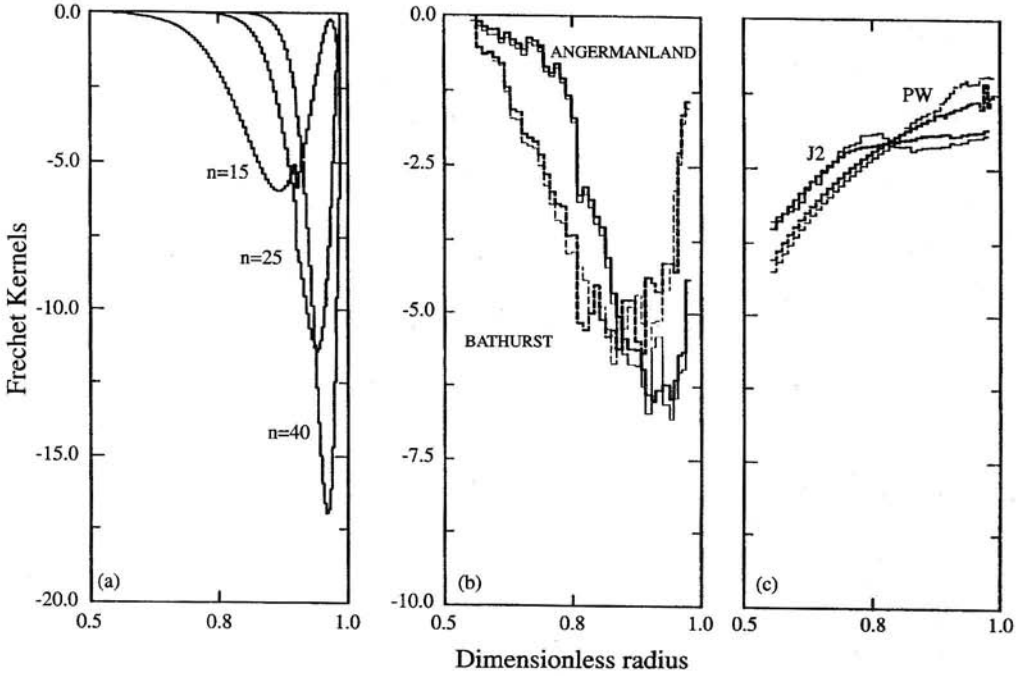

Fig. 8. Fréchet derivatives for a representative set of the data related to the GIA process. (**a**) shows a sequence of kernels for the inverse relaxation times of a number of spherical harmonic degrees of the McConnell relaxation spectrum based upon the analytical formula of Peltier (1976). (**b**) shows Frchet derivatives for the site-specific relaxation times at sites near the centre of Laurentide rebound (Bathurst Inlet; this is actually a high Arctic site) and at the center for Fennoscandian rebound (the Angerman River site). (**c**) shows kernels for the non-tidal acceleration of rotation ($\dot{J}_2$) and polar wander speed (PW) that were determined numerically using the procedure embodied in equations (8a) and (8b) of the text. Inspection of this suite of kernels, all of which were computed on model VM1, which is employed as starting model in the Bayesian inversions, demonstrates that the observables whose sensitivity to viscosity variations they represent offer the potential of significant resolution from the Earth's surface to the cmb.

the rsl record at Angerman River, which is located near the centre of Fennoscandian rebound. Also shown in this figure are the theoretically predicted spectra for the VM1, VM2 and VM3 viscosity models shown in Fig. 1. Inspection will show that the relaxation spectrum predicted by VM1 is such that relaxation times are too long at all spherical harmonic degrees, implying that upper-mantle and transition-zone viscosity is too high. That it is in fact the viscosity over this range of depths to which the Fennoscandian relaxation spectrum is sensitive is demonstrated in Fig. 8a, which shows Fréchet kernels for these relaxation time data for several values of the spherical harmonic degree, computed on the basis of the exact mathematical formula for them given by Peltier (1976). It will be clear by inspecting the spectrum for the VM2 model, also shown in Fig. 9, that the softer upper mantle and transition zone that characterize VM2 allow this model to fit the McConnell data extremely well.

The final set of data employed in the formal Bayesian construction of VM2 consists of a set of 21 relaxation times inferred on the basis of Monte Carlo fits of an assumed exponential uplift curve to individual rsl histories at sites that were once ice covered and at which the rsl records are distinctly exponential in form. Fifteen of these sites are in Canada and six in Sweden and Norway. These locations and the data from them are discussed in detail by Peltier (1996, 1998*b*). Examples of the Fréchet derivatives for such site-specific relaxation time data are shown in Fig. 8b for the Angerman River site in Sweden discussed previously and for the Bathurst Inlet site in the Canadian high Arctic. Inspection of these functions demonstrates that the rsl data controlled by the post-glacial recovery of the Laurentian platform are most sensitive to the viscosity in the upper part of the lower mantle, whereas those from Fennoscandia are most sensitive to shallower transition-zone structure.

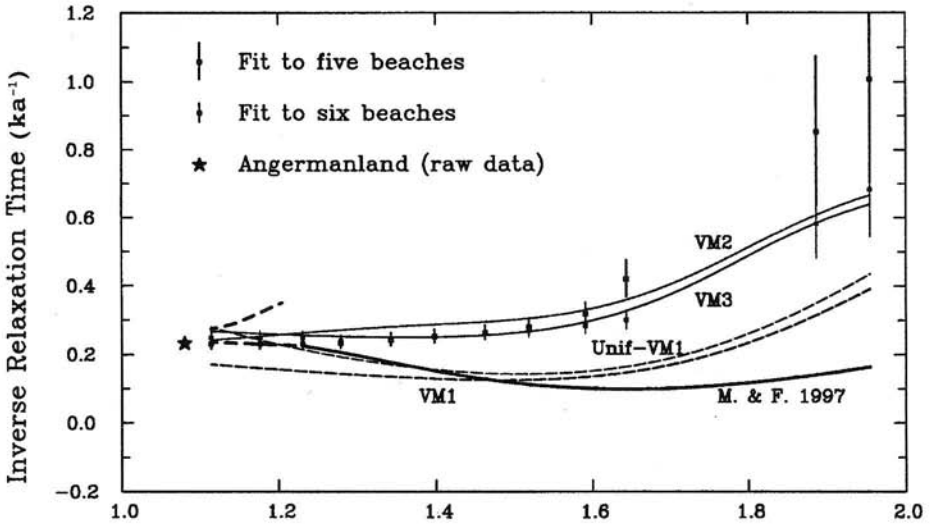

Fig. 9. The relaxation spectrum for Fennoscandian rebound of McConnell (1968) based upon both five and six strandline inversions. Also shown as the star symbol adjacent to the low wavenumber asymptote of the spectrum is the inverse relaxation time inferred from Monte Carlo fit to the rsl history at the Angerman River location, which is located near the centre of Fennoscandian rebound. Theoretical predictions of the spectrum are shown for models VM1, VM2 and VM3 in Fig. 1 as well as for model MF of Mitrovica & Forte (1997).

On the basis of this discussion it should now be clear why the formal Bayesian inversion of the totality of the above-described data deliver VM2 when VM1 is employed as the initial estimate. Because VM1 is too stiff in the upper mantle and transition zone to fit the McConnell spectrum, the viscosity in this region must be reduced. However, this reduction reduces the mean viscosity of the mantle, which is unacceptable to the rotational data. The latter data therefore require that the lower-mantle viscosity be increased to restore the mean value of viscosity to that in VM1. This adjustment occurs primarily in the lower part of the lower mantle because model VM1 fits the site-specific relaxation time data from the Hudson Bay region very well, meaning that the viscosity in the upper part of the lower mantle, to which these data are most sensitive (see Fig. 8), is held fixed near that in VM1, namely 2×10^{21} Pa s.

It will serve no useful purpose here to review the formal mathematical procedure employed in the Bayesian inversion which delivers VM2 from the VM1 first guess. The interested reader will find detailed discussions of this procedure in the studies by Tarantolla & Valette (1982, 1984), Jackson & Matsu'ura (1985) and Backus (1988). It will be useful, however, to end this discussion of the procedure employed to deduce the radial viscosity profile by illustrating the range of VM2-type models that may be derived by applying variations on the basic procedure. Examples of such profiles are shown in Fig. 10a and b. In Fig. 10a the two versions of VM2 differ from one another only because the site-specific relaxation time data employed in the inversion are deduced from the envelope sampled form of the rsl curves as in the archive of Tushingham & Peltier (1992) or from the raw age–height pairs directly. The former procedure leads to the version of VM2 shown as the heavy continuous line in Fig. 10a, whereas the latter procedure leads to the thin continuous line. These two variations of VM2 are clearly very close to one another. In Fig. 10b the raw data based version of VM2 from Fig. 10a is compared with a new version in which the forward predictions of the site-specific relaxation times were made using the version of the sea-level equation in which the full influence of time-dependent ocean function was included, an influence that was neglected in the inversions for which results are shown in Fig. 10a. Inspection of Fig. 10b will show that in this most accurate of the inversions the viscosity in the upper part of the lower mantle is somewhat elevated above 2×10^{21} Pa s but only very slightly. In this model the ratio of the viscosity in the upper part of the lower mantle to that in the upper mantle and transition zone is approximately five.

It will be useful to end this section with a very brief discussion of the relation between models in

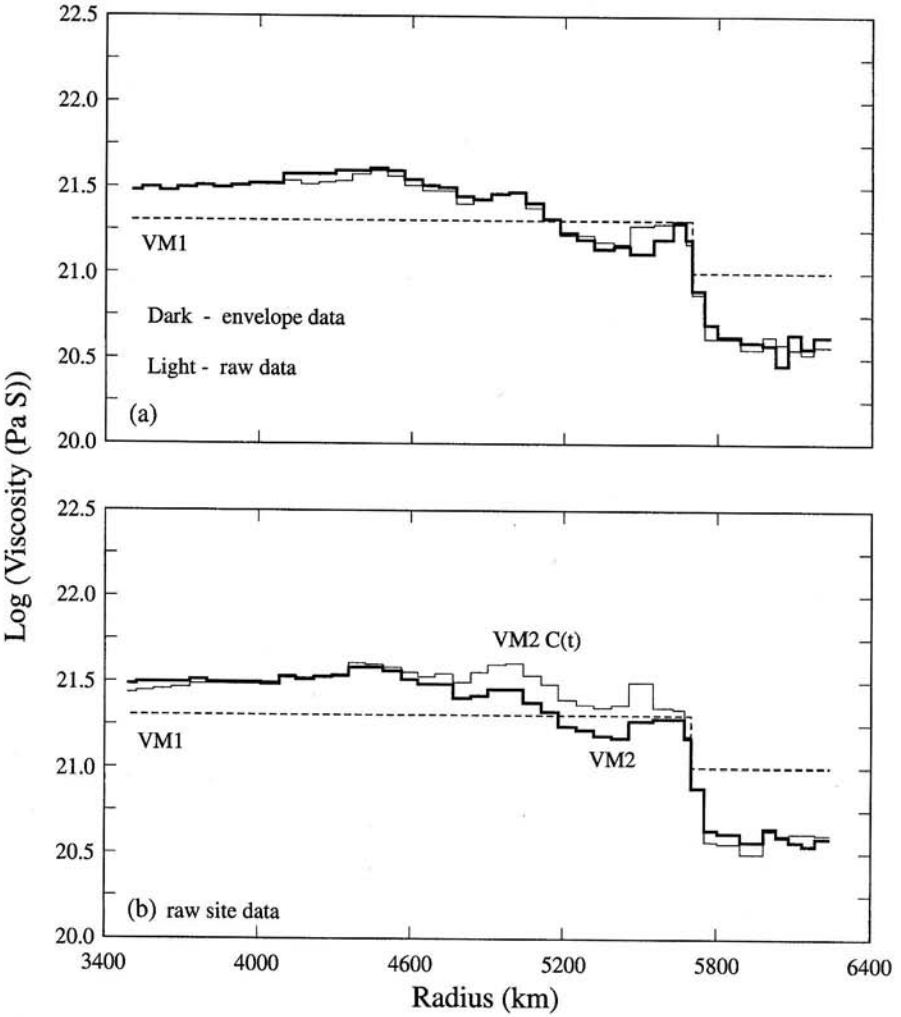

Fig. 10. Viscosity profiles determined by simultaneous formal Bayesian inversion of the Fennoscandian relaxation spectrum of McConnell (1968), the site-specific relaxation times from 23 ice-covered sites in Canada and Fennoscandia, and the non-tidal acceleration of the rate of axial rotation. In (**a**) the dashed line is the VM1 viscosity profile employed as starting model in the inversion process, and two versions of the final model are shown as the dark and light continuous lines, respectively, these being distinct versions of VM2. The former of these two inferred models has been obtained using site-specific relaxation times obtained from fits to the envelope sampled data compiled by Tushingham & Peltier (1992), whereas the latter was obtained on the basis of site-specific relaxation times deduced from the raw data themselves. In (**b**), where the dashed line again indicates VM1, the two versions shown are the final VM2 model (that based upon use of the raw data to determine the site-specific relaxation times) and a further version in which the starting model predictions were made with the version of the model that included the full influence of time dependence of the ocean function. Incorporation of the latter effect in the forward model slightly decreases the forward predictions for the site-specific relaxation times and therefore slightly increases the inferred viscosity in the upper part of the lower mantle, essentially back to the value of 2×10^{21} Pa s that is characteristic of the starting model VM1 in this region.

the class VM2 to those which have recently been advocated by other workers. The closest of these other models to VM2 is that derived by Lambeck *et al.* (1990) by trial-and-error fits to a set of rsl curves from Fennoscandia. Their model is identical to VM2 throughout the upper mantle and transition zone, approximately a factor of two higher in viscosity in the upper part of the lower-mantle (4.5×10^{21} Pa s), and essentially equal in the lower part of the lower mantle (in fact, these

workers quoted a range of allowed lower-mantle viscosities of $(2–7) \times 10^{21}$ Pa s). In the analyses presented herein, it is the data from the Hudson Bay region of Canada that collectively require the viscosity to be somewhat lower in the upper part of the lower mantle. Mitrovica & Peltier (1995) suggested that the site-specific rsl data from the Hudson Bay region exhibit a significant spread in relaxation times ranging from a low near 2000 years (Ottawa Islands) to a high near 7600 years (Richmond Gulf). Advocates of higher values of viscosity in the upper part of the lower mantle than that in VM2 (e.g. Mitrovica 1996; Forte & Mitrovica 1996; Mitrovica & Forte 1997; Simons & Hager 1997; to be referred to collectively in what follows as MFSH) have focused entirely upon the Richmond Gulf record and ignore all the rest, an approach which introduces significant bias as there is no reason to believe that the Richmond Gulf record is superior to any of the others. It has, in fact, become clear in the course of recent analyses (Peltier 1998*c*) that the previously published high estimate of the relaxation time at Richmond Gulf (Mitrovica & Peltier 1995) is in error. Rather than being near 7600 years as suggested by Mitrovica & Peltier (1995), it is in fact best estimated as 3400 ± 400 years on the basis of a complete reanalysis of all available ^{14}C data from the southeast Hudson Bay region when these are properly transformed onto the sidereal timescale using the Calib. 3.0 software of Stuiver & Reimer (1993). The VM2 model

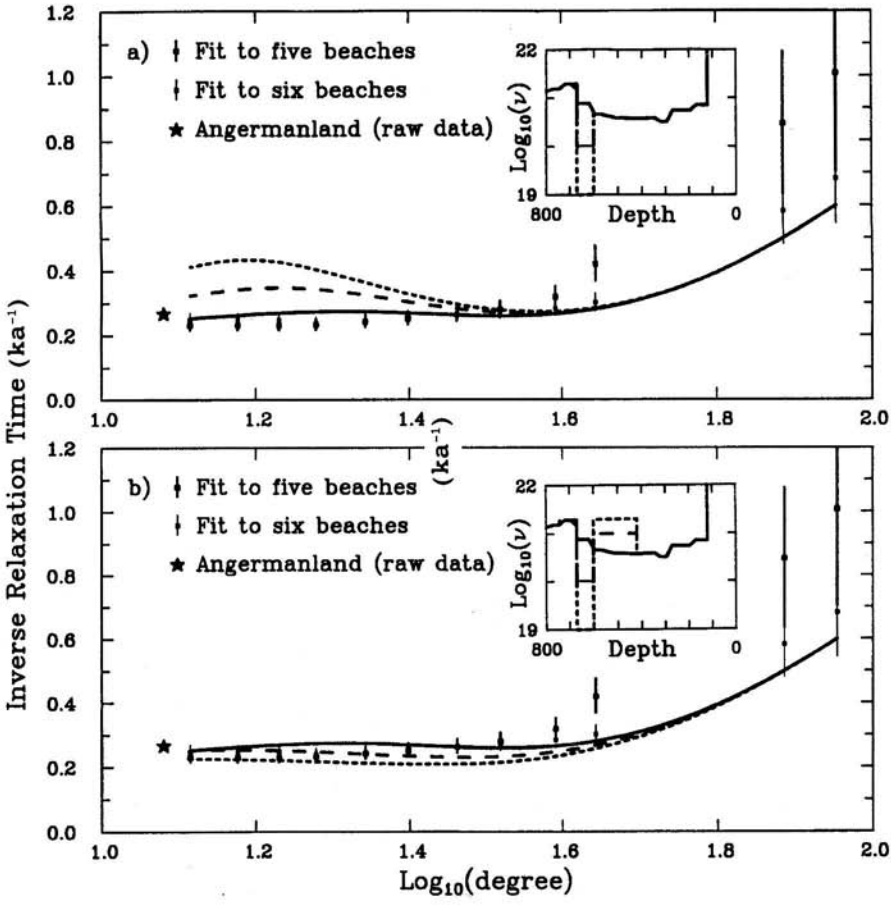

Fig. 11. (a) The inverse relaxation time spectrum for Fennoscandian rebound of McConnell (1968) compared with the prediction of a model in the VM2 class and compared with the predictions for two additional models that differ from VM2 by the presence of a 70 km thick layer immediately overlying the 660 km discontinuity in which the viscosity is reduced either by one or two orders of magnitude from the value near 0.45×10^{21} Pa s that otherwise obtains in this region of VM2.

predicts precisely this relaxation time in south-east Hudson Bay near the centre of uplift. It is therefore clear on this basis that the inferences of viscosity presented by MFSH are untenable. Further evidence of this fact is clear on the basis of analysis of the upper-mantle and transition-zone viscosity structures of the MFSH models. Those models of the shallow structure include both extremely soft transition zones and higher-viscosity upper mantles. Structures of this kind would appear to be ruled out entirely by the McConnell (1968) spectrum for Fennoscandia rebound as demonstrated in Fig. 9, where the spectrum of the Mitrovica & Forte model (denoted MF) is compared with those of the VMX models as well as with McConnell's data. If models of this type are to be entertained it is clearly incumbent upon their advocates to prove that the McConnell (1968) spectrum is very significantly in error. Otherwise the VM2 model must be strongly preferred, a model which is similar to that earlier advocated by Lambeck *et al.* (1990) although with significantly lower contrast in viscosity across the spinel–post spinel phase transition at 660 km depth.

It is very important to realize, however, that the VM2 family of models may in no sense be construed to represent a 'uniquely' preferred solution to the one-dimensional mantle viscosity inverse problem. Although one can argue this point formally, it is probably more useful to demonstrate it by providing a specific example. To this end, Fig. 11a shows results for the McConnell spectrum obtained using a perturbed version of the VM2 profile in which a thin low-viscosity layer is inserted into the structure immediately above the 660 km seismic discontinuity, with the viscosity in this layer being fixed to either 10^{20} Pa s or 10^{19} Pa s. The presence of such a structure has been inferred to be required in viscosity models derived by inversion of the non-hydrostatic geoid anomalies that are supported by the mantle convection process (e.g. Forte *et al.* 1993*a*, *b*; Pari & Peltier 1995). Even though models of the perturbed kind shown in Fig. 11a are essentially identical with those required by these data, insofar as the radial variation of viscosity is concerned, it is clear that such models do not fit the McConnell (1968) relaxation spectrum and they are therefore untenable insofar as the GIA data are concerned. However, it is possible to further perturb the structure so as to recover the good fit to the McConnell spectrum as shown in Fig. 11b. The results shown in this figure demonstrate that the presence of the soft layer may be easily accommodated simply by increasing the viscosity of the rest of the transition zone back towards the value in VM1, namely 10^{21} Pa s. Models of this kind would not be ruled out by the data yet they differ significantly from VM2. As the transition zone is rich in garnet and as this mineral has a high creep resistance, one may be tempted to argue that such models are actually to be preferred. For present purposes, however, these analyses are presented simply to demonstrate the extreme degree of non-uniqueness in the radial variation of viscosity that the data allow.

Model–data intercomparisons for rsl history

As discussed in the last section, very few of the rsl data that are actually available have been employed to tune the radial viscosity profile of the model; in fact, the only data used in this way are those from sites located near the centres of the Laurentian and Fennoscandian ice sheets, and from Barbados, where the coral-based record of Fairbanks (1989), which extends to LGM, has been used to constrain the total ice melt in the deglaciation model. All of the remaining data may therefore be employed to verify the quality of the ICE-4G (VM2) model. In the discussion to follow, the focus of the first subsection will be upon rsl data that actually constrain the time-dependent elevation of the shoreline and that usually derive from ^{14}C dating of mollusc shells or wood specimens whose indicative meaning in the landscape suggests that the sample records a former level of the sea. In the second subsection the focus will shift to the U/Th-dated coral records of rsl history mentioned in the Introduction.

Relative sea-level histories beyond the ice sheet margins

The ^{14}C data that will be employed in this subsection to test the quality of the ICE-4G (VM2) model constitute an extremely small subset of the *c.* 600 individual rsl records that are now contained in the database at the University of Toronto. This database has yet to be published and constitutes a considerable improvement upon the reconnaissance collection of Tushingham & Peltier (1991, 1992). Rather than being based upon sampling the envelope of the set of age–height pairs that are derived from each sample, the new data base consists of the raw data themselves and it is these data that will be employed for comparison purposes herein. When these data are compared with the predictions of the theoretical model we must of course transform from ^{14}C time to sidereal time, and for this purpose we employ the Calib. 3.0 program of Stuiver & Reimer (1993), which links the extensive tree ring database for the

Holocene to the coral-based U/Th calibration of Bard *et al.* (1990) for the late glacial period.

One of the most important regions in which the model may be subjected to rigorous test comprises the entire eastern seaboard of the continental USA. This is because even the earliest analyses based upon the VM1 model (Peltier *et al.* 1986; Tushingham & Peltier 1992) demonstrated that there were significant misfits between the observations and the predictions such that the rates of sea-level rise predicted to be occurring as a result of the collapse of the proglacial forebulge were much higher than observed in this geographical region. That these misfits are essentially completely eliminated by ICE-4G (VM2) is demonstrated in Fig. 12, which compares observations with theoretical predictions at Montreal, Quebec (which was located just inside the ice sheet margin), Boston, Massachusetts (which was located very close to the ice sheet margin itself), Brigantine, New Jersey (which was located outboard of the ice sheet near the crest of the forebulge) and Lilliput Creek, North Carolina. All of these data are well fitted by the theoretical predictions, demonstrating, as previously documented by Peltier (1996), that the previously evident misfits are eliminated. This is rather important because the modification to VM1 to produce VM2 primarily involves a reduction of the creep resistance in the upper mantle and transition zone that was required to fit the rsl data from Fennoscandia. As this modification to the structure also allows the model to reconcile North American data, this suggests that the upper-mantle and transition-zone viscosity below North America are essentially the same as beneath Northwestern Europe. A global representation of the marked difference in the rsl history predicted by the VM1 and VM2 viscosity models when the ICE-4G deglaciation history is employed in the calculation is provided in Fig. 13, which shows the present-day predicted rate of rsl rise for both models as well as the difference between them. The difference between these predictions is clearly largest along the US east coast, in precisely the region where the misfits of the VM1-based theory to the observations were largest.

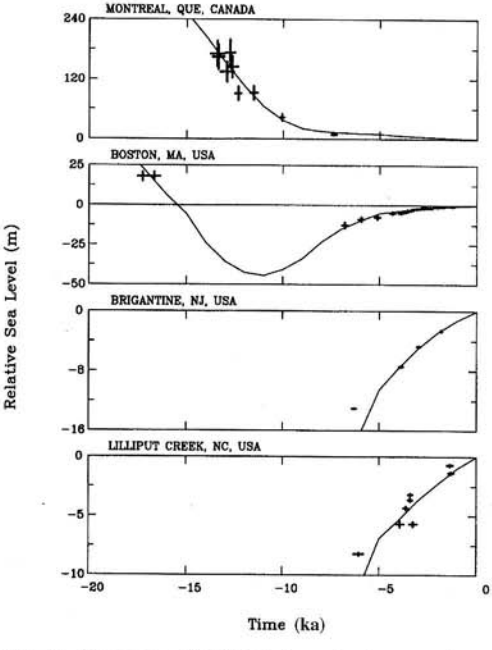

Fig. 12. Examples of ^{14}C-dated sea-level curves from four sites on the east coast of the North American continent: Montreal (Quebec) in Canada, and Boston (Massachusetts), Brigantine (New Jersey) and Lilliput Creek (North Carolina) in the USA. The carbon dates for the individual samples have been converted to sidereal years using the U/Th-based calibration of Stuiwer & Reiner (1993) and the raw data, corrected in this way, are compared with the predictions of the ICE-4G (VM2) model.

Probably the best location in the world from the perspective of the quality of the post-glacial rsl data that are available from it, however, is the British Isles. This region is also especially interesting because it is not only located in the region of forebulge collapse that surrounds the previously glaciated region of Fennoscandia but it was also glaciated in the north, where a significant mass of ice was located over the highlands of Scotland. Furthermore, the coastline of this region experienced significant variation subsequent to LGM, when a vast land bridge connected Britain to France. Figure 14 shows the locations of four sites from which high-quality rsl data are available, superimposed upon the inundation map which illustrates the way in which the coastline is predicted to have evolved based upon the ICE-4G (VM2) model. Figure 15 compares predicted and observed rsl history at Tay Valley and North Solway Firth, Scotland, both sites in the northern region that was once ice covered, and at the Fenlands and Bristol Channel locations in the south, which remained ice free. Inspection of these comparisons clearly demonstrates that the ICE-4G (VM2) model very accurately predicts even the very complex and highly non-monotonic rsl histories that obtained in the northern region, where a complex interplay occurs between the process of post-glacial rebound of the crust that causes sea level to fall and rising sea levels caused by the melting of distant ice sheets. The

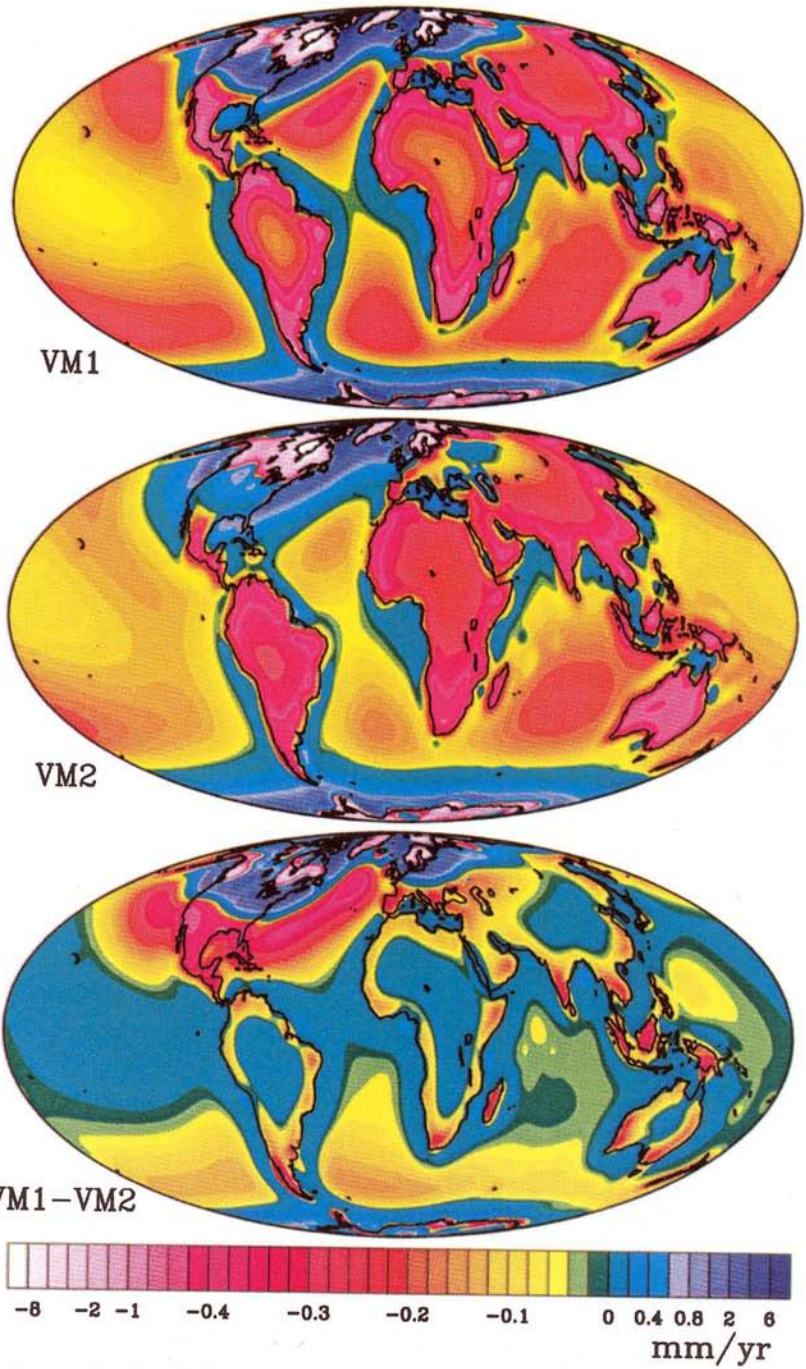

Fig. 13. Present-day rates of sea-level rise predicted using the VM1 and VM2 viscosity models in conjunction with the ICE-4G deglaciation history. The difference between the predictions of these models is maximum along the US east coast, as shown in the final part of the figure.

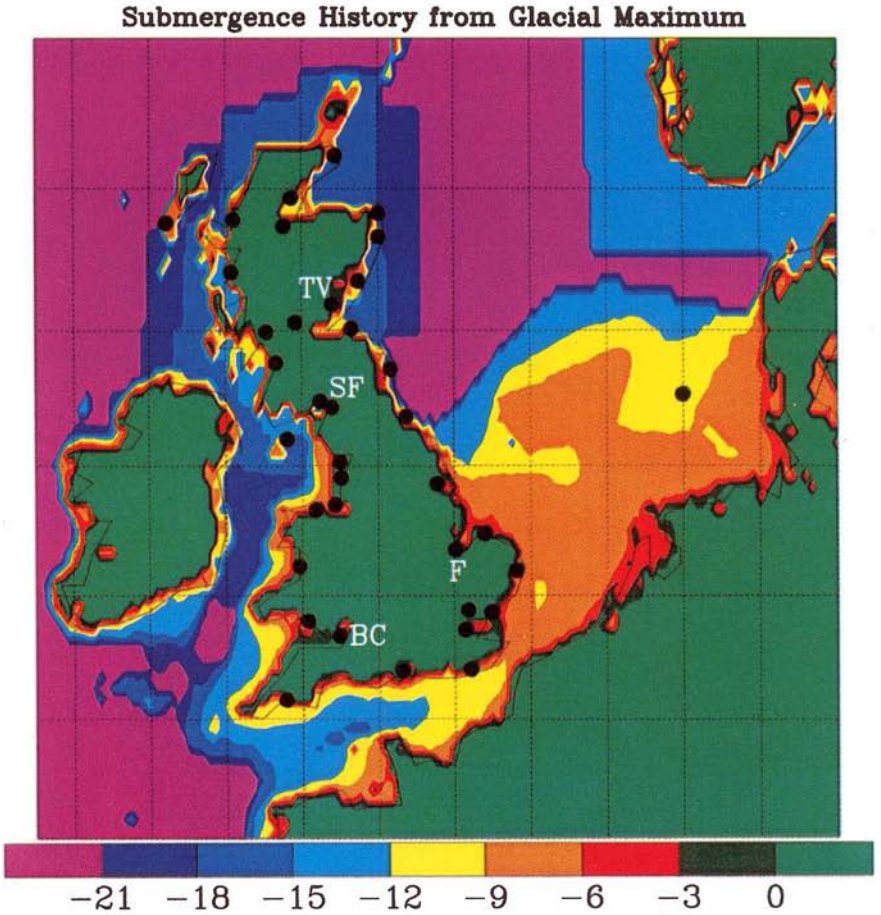

Fig. 14. Inundation map for the British Isles on which are superimposed the locations of the two sites in Scotland and the two sites in England for which the rsl data are described in the text. TV, Tay Valley; SF, Solway Firth; F, Fenlands; BC, Bristol Channel.

fact that the ICE-4G (VM2) model fits these data extremely well is important because it has been previously argued that the data from this region required a rather high value of the viscosity of the lower mantle, in fact near 10^{22} Pa s (Lambeck *et al.* 1996), and therefore considerably in excess of the viscosity over the same range of depths that had been inferred previously on the basis of rsl records from the immediately adjacent Fennoscandia region (Lambeck *et al.* 1990). Clearly, models with such large radial viscosity contrasts are not, in fact, required by the data from the British Isles. The interested reader will find a far more detailed discussion of the post-glacial sea-level history of the British Isles in the study by Peltier & Shennan (1998).

Moving further still away from the main centres of glaciation into the region that I have previously referred to as the 'far field' of the ice sheets, Fig. 16 compares predicted and observed rsl histories at a sequence of sites that extends from the Caribbean Sea along the east coast of the South American continent to the northern part of Argentina. The first plate in this sequence once more reproduces the fit to the U/Th-dated coral sequence from Barbados, a record that was actually employed to tune the ice load component of the model (Peltier 1994) as mentioned previously. Moving further south to Recife and Santos–Itanhaem, in Brazil, and Bahia Solano, in Argentina, we note that the most apparent characteristic of the records of rsl history, both observed and predicted, is the existence of a

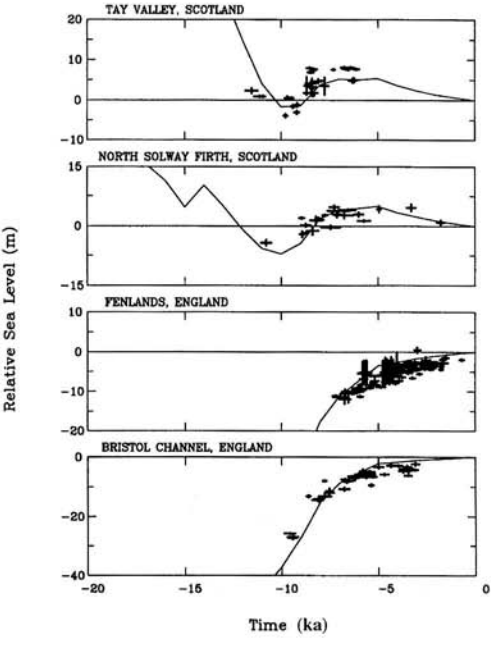

Fig. 15. Examples of ^{14}C-dated rsl curves from four sites in the British Isles: Tay Valley and Solway Firth in the once ice-covered region of Scotland, and the Fenlands and Bristol Channel, which were both beyond the southernmost extent of the Scottish ice sheet. As discussed in the text, the records from Scotland are highly non-monotonic, because of the superimposition at these locations of the influence of rebound of the crust owing to ice removal and the influence of the collapse of the Fennoscandian forebulge and continuing addition of mass to the oceans caused by the melting of both Laurentide and Fennoscandian ice.

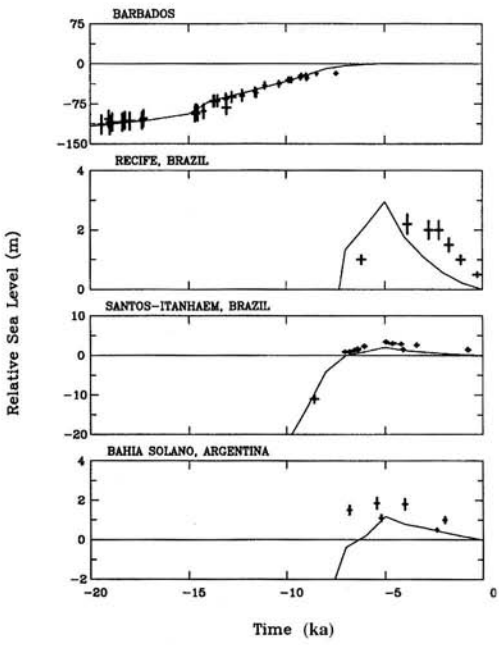

Fig. 16. Examples of ^{14}C-dated sea-level curves from four sites along the east coast of the South American continent from Barbados in the north to Recife and Santos–Itanhaem on the coast of Brazil, and to Bahia Solano in Argentina. It is interesting to note that although the data from the northern sector of the coast are fairly well fitted by the ICE-4G (VM2) based theory, as one moves further to the south the data show increasing evidence of the action of the influence of tectonic uplift (a detailed analysis of this tilting effect will be provided elsewhere).

mid-Holocene high stand that occurs at *c.* 5 ka BP. The fit to the observed highstand is excellent at Santos–Itanhaem, acceptable at Bahia Solano but less so at Recife where a significant phase shift appears to exist. As will be discussed in detail elsewhere, the southernmost east coast of Argentina, Patagonia, appears to be experiencing some tectonic uplift, presumably because of the increasingly close proximity to the Chile trench as one moves further southwards along the east coast.

In the final sequence of intercomparisons, shown in Fig. 17, the mid-Holocene highstand of sea level continues to be the most prominent feature of the records of rsl history. These records are all from the Pacific Ocean sector, and from north to south correspond to Osaka Bay, Japan, Rota Island in the Marianas, Balding Bay, Australia, and Christchurch, New Zealand. The theoretical prediction of the sea-level history at each of these locations is again dominated by the existence of a mid-Holocene highstand with maximum height above present sea-level occurring at *c.* 5 ka BP and achieving an amplitude of *c.* 2 m. As previously mentioned, it was the prediction of this feature which is extremely well expressed across the entire Pacific Ocean, that attracted such attention to this work when solutions of the sea-level equation were first reported by Clark *et al.* (1978) and Peltier *et al.* (1978). A more recent discussion of the data that constrain this feature from the archive of Tushingham & Peltier (1992) was presented by Mitrovica & Peltier (1991). All of these records, most of which are constrained by a very small number of data points, are reasonably well explained by the theory. In the next subsection, we will consider a series of records which have been construed to pose a considerable challenge to the global theory.

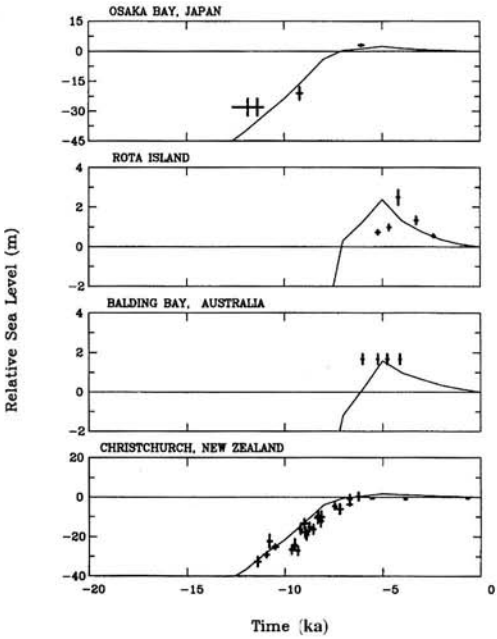

Fig. 17. Examples of ^{14}C-dated sea-level curves from four sites in and on the margin of the Pacific Ocean, ranging from Osaka Bay in the north to Christchurch, New Zealand, in the south. At the intermediate sites of Rota Island and Balding Bay, Australia, the mid-Holocene highstand of sea level is especially apparent.

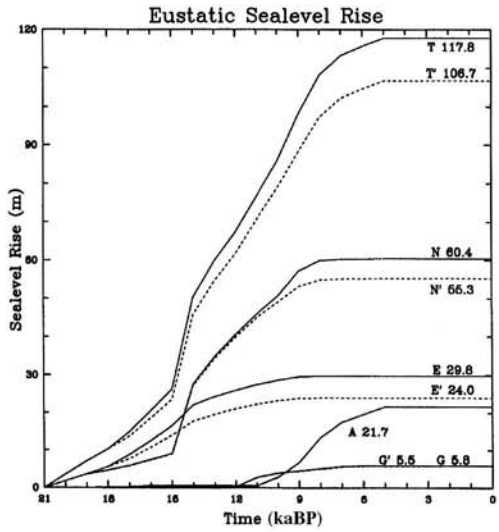

Fig. 18. The total eustatic sea-level rise is shown from the model that both excludes (T′) and includes (T) the influence of implicit ice as discussed in the text in connection with equations (14)–(16). Also shown are the individual contributions from North America (N, N′), Eurasia (E, E′), Antarctica (A) and Greenland (G, G′).

Coral-based records of rsl change: the Pacific Ocean sector

At several points in the above discussion, I have drawn attention to the fact that the ICE-4G (VM2) model was tuned in terms of the total ice amount so that it would fit the U/Th-dated coral-based rsl record from Barbados. The reason for focusing upon this record is that it is unique from a number of points of view. First, it is the only accurately dated rsl record which extends back to LGM and which therefore can be used to constrain the amount by which sea level rose from that time to the present. Second, however, is the fact that this record is composed almost entirely of age–depth measurements on the coral species *Aquapora palmata*. As this Caribbean species is known to live at a depth that is within 5 m of sea level, this record may be assumed to constitute a good recording of changing sea level itself. Of course, it is also well known that Barbados is rising at a rate that is usually assumed to be near 0.35 mm per year, implying that to derive actual sea level from the raw age–depth data for the Barbados sequence one needs to make a tectonic correction. The magnitude of this correction is therefore such as to require sea level to have risen at Barbados since LGM by *c.* 7 m more than suggested by the raw data. The position that I will adopt for present purposes, as I have done in the past, is that if the theoretically predicted rsl history at Barbados is such that the prediction goes through the raw data points themselves then, given the observed range of living depths of *A. palmata*, no further correction to the data is required. This is particularly true as the best estimate of the rate of tectonic uplift at Barbados is probably closer to 0.25 mm per year than to 0.35 mm per year. The fit of the ICE-4G (VM2) model to the Barbados data has been shown previously in Figs 4 and 14, where the predicted rise of sea level at this location is seen to be just slightly less than 120 m. It is important to note that this is slightly greater than one might expect based upon the net mass of 'explicit' ice that is melted across the glacial–interglacial transition, though one must remember that determination of the rise of sea level at any given site requires a correction to the effect expected on the basis of mass alone (see equations (4) and (5)). The sea-level rise based upon the consideration of ice-mass alone (both explicit and implicit as discussed previously), for each of the main sectors in which melting occurs, is shown in Fig. 18,

inspection of which shows that one would expect sea level to rise by only 106.7 m if only the explicit ice melted in ICE-4G were to be added uniformly to ocean basins of fixed present-day area. On the other hand, when the influence of implicit ice is properly taken into account, the discrepancy is much reduced, as the predicted total eustatic rise increases to 117.8 m.

Figure 19 shows the locations of the additional sites in the Pacific basin that will be of interest for the remainder of this subsection, namely, the Huon Peninsula of Papua New Guinea, Tahiti and Sumba and Morley Islands. At each of these locations coral-based records of rsl change are also available for which the age control is based upon U/Th dating (Edwards 1988). It is clearly interesting to enquire as to whether or not the global theory is also able to reconcile these additional observations, the most important of which are probably those from the Huon Peninsula (Edwards 1988; Chappell & Pollach 1991; Ota *et al.* 1993). On the basis of their observations of the uplifted Pleistocene interglacial terraces near the Kwambu–Kilasairo location, Chappell & Polach (1991) inferred a late Pleistocene average rate of tectonic uplift at Huon of 1.9 mm per year. In Fig. 20a, I show not only the raw data for Huon but also the corrected data when this rate of tectonic uplift is employed to reduce them, along with the theoretical prediction based upon the ICE-4G (VM2) model. Whereas the raw data lie somewhat above the theoretical prediction at young age, it is clear that when the data are corrected by assuming the conventional rate of tectonic uplift they lie considerably below the theory, so far below as to suggest that perhaps the theory may be in error (see comments by Edwards (1995)). Also shown in Fig. 20, however, are comparisons between observations and theoretical prediction

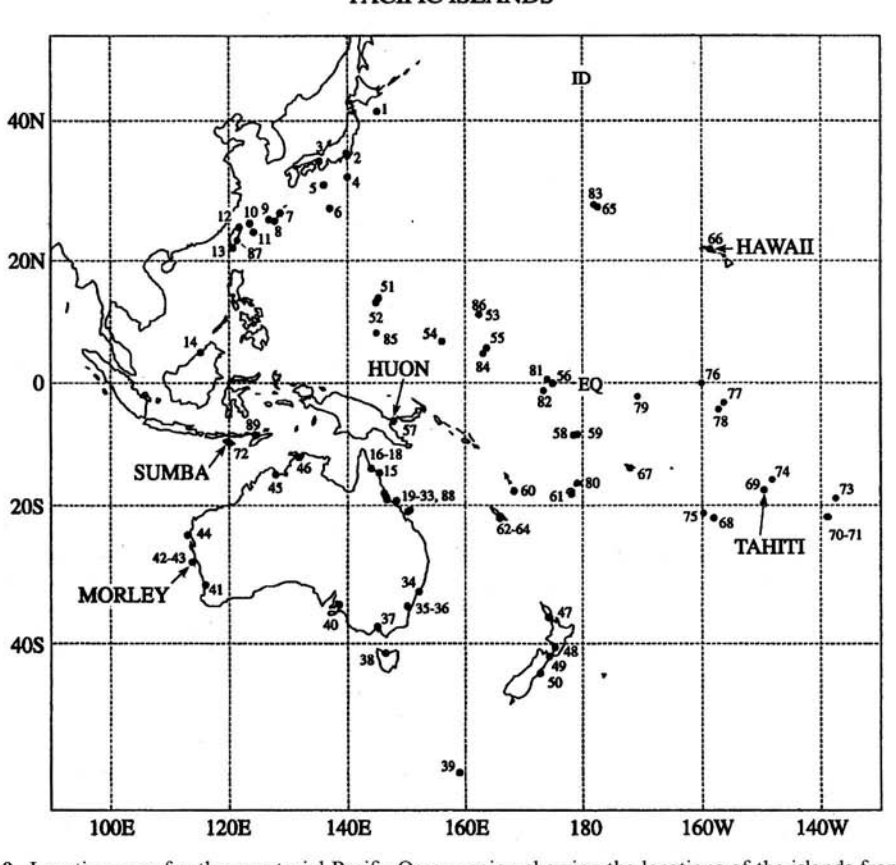

Fig. 19. Location map for the equatorial Pacific Ocean region showing the locations of the islands from which information on rsl history is available. The data from those islands for which names are given are discussed in the text. The numbering scheme for the other locations is that employed in the global recompilation of rsl data that has been continuing at Toronto for the past several years.

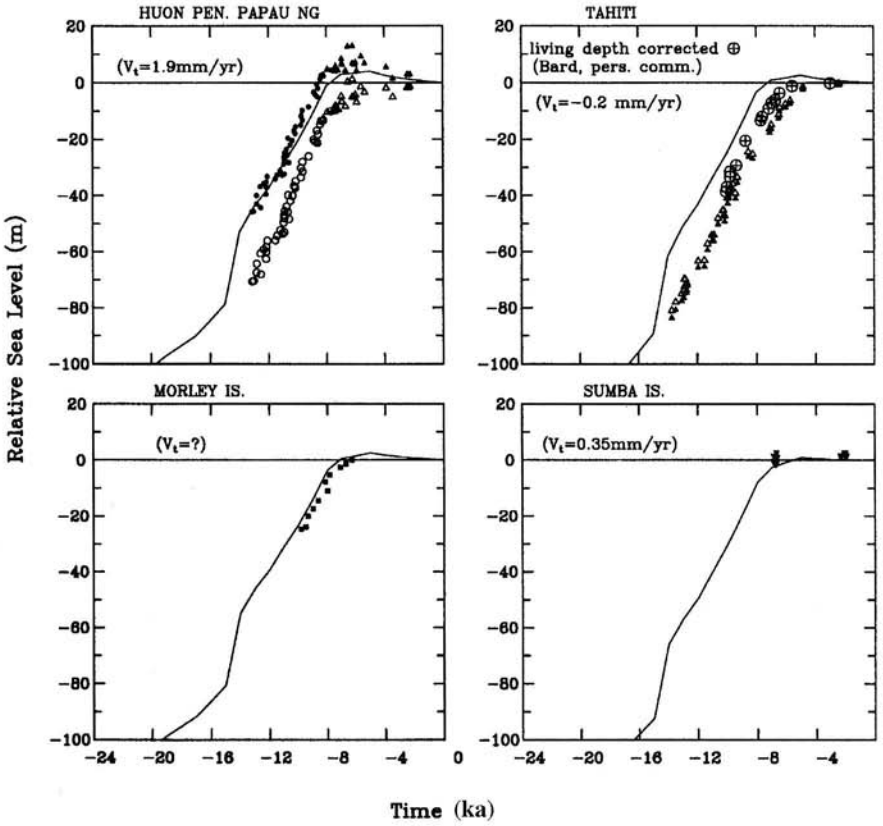

Fig. 20. The raw and tectonic uplift corrected coral-based records are shown, along with the predicted sea-level histories based upon model ICE-4G (VM2) for (**a**) the Huon Peninsula, (**b**) Papeete Harbour, Tahiti, (**c**) Morley Island and (**d**) Sumba Island.

for the rsl history at Morley Island (Eisenhauer *et al.* 1993) and Sumba Island (Bard *et al.* 1996*b*), whose locations are also shown in Fig. 19. Inspection of the intercomparisons at these sites demonstrates that at these locations theory and observations agree rather well, although in the case of Sumba Island the data are sparse (essentially only two points). At Sumba there is an estimate, noted in the figure, of the rate of tectonic uplift active at this location, and it will be noted that when this correction is applied to the data the fit of the two data points to the theory is excellent. At Morley Island the observations and theory agree very well if allowance is made for a small living depth correction. Both of these additional datasets are consistent with the existence of a mid-Holocene highstand in the sea-level record but neither data set actually resolves the feature.

It is nevertheless clear that when the Huon data are 'corrected' by assuming that the conventional Pleistocene rate of tectonic uplift also applies during the Holocene period then the fit of the theory to the data is anomalous in that it is so poor. The most apparent anomaly concerns the absence of the mid-Holocene highstand in the rsl record when the 1.9 mm per year tectonic uplift rate is used to make the correction. It seems clear on this basis that the 1.9 mm per year average rate of Pleistocene uplift at the Kwambu–Kilasairo site on the Huon Penninsula is not characteristic of the Holocene period. To determine the rate that has actually been characteristic of this most recent epoch we might best proceed by asking what is the rate that must be assumed to minimize the misfit between observations and theoretical prediction. The results of this analysis are shown in Fig. 21. Depending upon whether one minimizes the misfit over the entire dataset or only over the last 9000 years one infers a best rate of tectonic uplift between 0.3 and 0.65 mm per year, although the minimum in variance is rather flat so that the rate is not accurately determined. As suggested by Peltier

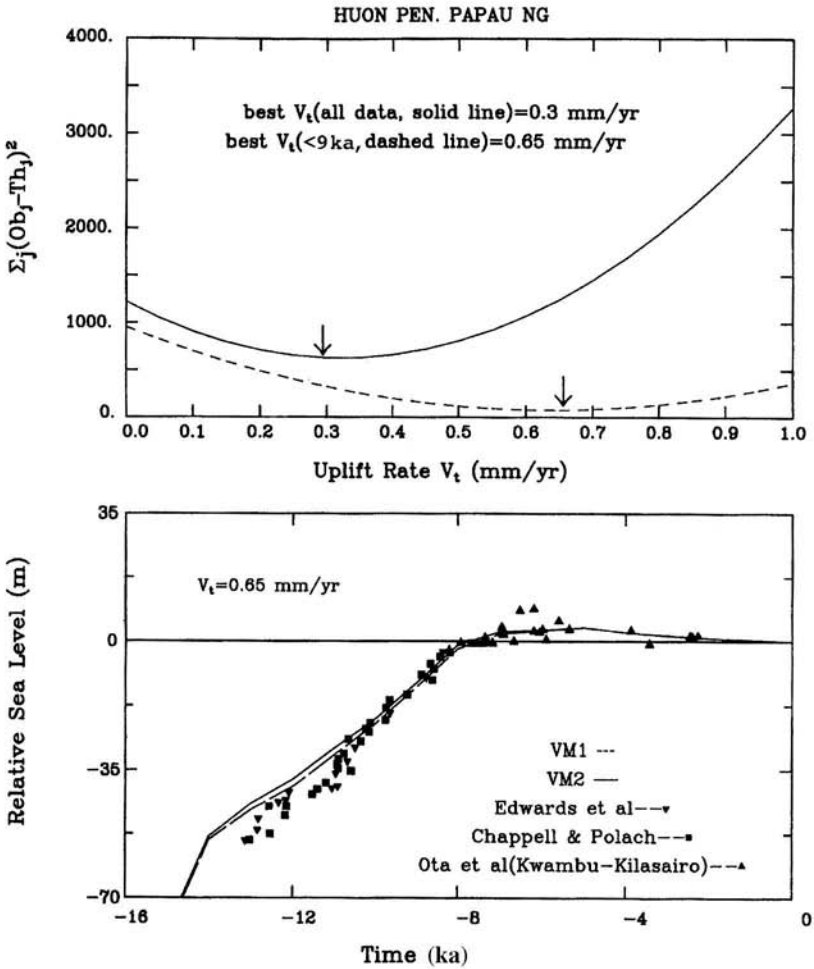

Fig. 21. (**a**) Variance reduction between the prediction of the rsl history on the Huon Peninsula for the ICE-4G (VM2) model and the observations as a function of the rate of tectonic uplift assumed for the purpose of correcting the observations. Variance reduction is shown based upon the use of all available data and the use of only data younger than 9 ka. With the former assumption the 'best-fitting' rate of tectonic uplift is found to be 0.35 mm per year. (**b**) Fit of the tectonically corrected data to the ICE-4G (VM2) prediction.

(1995), it therefore seems clear that the rate of tectonic uplift at Huon during the Holocene period has been much less than the Pleistocene average rate.

One final piece of analysis that warrants discussion here, concerning the tectonic contribution to Holocene sea-level history, relates to the data for Tahiti (Bard *et al.* 1996*a*), which are also shown in Fig. 19. At Tahiti, unlike at Huon, the theoretically predicted rsl history delivered by the ICE-4G (VM2) model lies above the observations rather than below. However, rather than being subject to tectonic uplift, Tahiti is subject to tectonic subsidence. This is perhaps primarily a consequence of the fact that the island is emplaced in lithosphere that sinks is it cools while moving away from the East Pacific Rise at a rate near 12 cm per year. Now the rate of subsidence that has been suggested to be characteristic of Tahiti is near 0.2 mm per year, but when this correction is applied to the data it does not significantly improve the fit to the observations. When an additional correction is made for the influence of living depth (E. Bard, pers. comm.) the misfit is further reduced (see the figure). However, the data still do not contain the clearly evident mid-Holocene highstand of sea level that is observed to be characteristic of all rsl data from far field locations. Further analysis of the data at Tahiti is clearly warranted.

On the basis of all of the data discussed in this subsection, it is clear that when the model is tuned to fit the history of post-glacial sea-level change at Barbados, as well as those from ice-covered sites, then the model also fits far field rsl histories at locations that were not employed to tune the model parameters. The model must therefore be considered highly successful.

Conclusions

In the previous sections of this paper, I have both reviewed and extended the global theory of post-glacial sea-level change that has been developed over the past two decades. This theory is now rather fully articulated and has been shown to reconcile a wide range of geophysical and geological data. One of the most active areas of current application involves the investigation of the extent to which space geodetic data may be brought to bear to further constrain model parameters. Three different types of such data have now been shown to be useful adjuncts to the geological and astronomical measurements that have been the conventional focus in such work. These consist of observations of the non-tidal acceleration of axial rotation based upon the use of LAGEOS satellite laser ranging data (Peltier 1983; Yoder *et al.* 1983), observations of the rate of radial displacement based upon the use of VLBI observations (Argus 1996) and, most recently, observation of tangential motions associated with the GIA process based upon global positioning system (GPS) observations (BIFROST 1997). Application of these measurement systems is expected to prove to be especially useful in understanding the relative contributions of tectonics and glacial isostasy to individual records of rsl history.

References

ARGUS, D. F. 1996. Postglacial rebound from VLBI geodesy: on establishing vertical reference. *Geophysical Research Letters*, **23**, 973–977.

BACKUS, G. E. 1988. Bayesian inference in geomagnetism. *Geophysical Journal of the Royal Astronomical Society*, **92**, 125–142.

BARD, E., HAMELIN, B., ARNOLD, M., MONAGGIONI, L., CABIOCH, G., FAURE, G. & ROUGERIE, F. 1996*a*. Deglacial sea level record from Tahiti corals and the timing of global meltwater discharge. *Nature*, **382**, 241–244.

——, ——, FAIRBANKS, R. G. & ZINDLER, A. 1990. Calibration of the ^{14}C timescale over the past 30,000 years using mass spectrometric U–Th ages from Barbados corals. *Nature*, **345**, 405–409.

BARD, E., JOHANNIC, C. *et al.* 1996*b*. Pleistocene sea levels and tectonic uplift based on dating of corals from Sumba Island Indonesia. *Geophysical Research Letters*, **23**, 1473–1476.

BIFROST 1996. GPS measurement to constrain geodynamic processes in Fennoscandia. *EOS Transactions of the American Geophysical Union*, **35**, 377.

BILLS, B. G. & JAMES, T. S. 1996. Late Quaternary variations in relative sea level due to glacial cycle polar wander. *Geophysical Research Letters*, **23**, 3023–3026.

CHAPPELL, J. & POLACH, H. A. 1991. Post-glacial sea level rise from a coral record at Huon Peninsula, Papua New Guinea. *Nature*, **276**, 602–604.

CLARK, J. A., FARRELL, W. E. & PELTIER, W. R. 1978. Global changes in postglacial sea level: a numerical calculation. *Quaternary Research*, **9**, 265–287.

DAHLEN, F. A. 1976. The passive influence of the oceans upon the rotation of the Earth. *Geophysical Journal of the Royal Astronomical Society*, **46**, 363–406.

DZIEWONSKI, A. M. & ANDERSON, D. L. 1981. Preliminary reference earth model. *Physics of the Earth Planetary Interiors*, **25**, 297–356.

EDWARDS, R. L. 1988. *High precision Th-230 ages of corals and the timing of sea level fluctuations in the late Quaternary*. PhD Thesis, California Institute of Technology, Pasadena.

——1995. Paleotopography of Ice-Age ice sheets. *Science*, **267**, 535–536.

EISENHAUER, A., WASSERBURG, G. J., CHEN, J. H., BONANI, G., COLLINS, L. B., ZHU, Z. R. & WYRWOLL, K. H. 1993. Holocene sea level determination relative to the Australian continent: U–Th (TIMS) and ^{14}C (AMS) dating of coral cores from the Abrolhos Islands. *Earth Planetary Science Letters*, **114**, 529–547.

FAIRBANKS, R. G. 1989. A 17,000-year glacio-eustatic sea level record: influence of glacial melting rates on the Younger Dryas event and deep-ocean circulation. *Nature*, **342**, 637–641.

FANG, M. & HAGER, B. H. 1995. The singularity mystery associated with radially continuous Maxwell viscoelastic structure. *Geophysical Journal International*, **123**, 849–865.

FARRELL, W. E. & CLARK, J. A. 1976. On postglacial sea level. *Geophysical Journal of the Royal Astronomical Society*, **46**, 647–667.

FORTE, A. M., DZIEWONSKI, A. M. & WOODWARD, R. L. 1993*a*. Aspherical structure of the mantle, tectonic plate motions, nonhydrostatic geoid and topography of the core–mantle boundary. *In*: LE MOUEL, J.-L. (ed.) *Dynamics of the Earth's Deep Interior and Earth Rotation*, Geophysical Monograph Series, American Geophysical Union, **72**, 135–166.

——, PELTIER, W. R., DZIEWONSKI, A. M. & WOODWARD, R. L. 1993*b*. Earth's dynamics topography: a new interpretation based upon mantle flow models derived from seismic tomography. *Geophysical Research Letters*, **20**, 225–228.

HAN, D. & WAHR, J. 1995. The visco-elastic relaxation of a realistically stratified Earth, and a further analysis of postglacial rebound. *Geophysical Journal International*, **120**, 287–311.

HAYS, J. D., IMBRIE, J. & SHACKLETON, N. J. 1976. Variations in the Earth's orbit: pacemaker of the ice ages. *Science*, **194**, 1121–1132.

IMBRIE, J., HAYS, J. D. *et al.* 1984. The orbital theory of Pleistocene climate: support from a revised chronology of the marine $\delta^{18}O$ record. *In*: BERGER, A. L. *et al.* (eds) *Milankovitch and Climate, Part 1*, D. Reidel Publishing Company, 269–305.

JACKSON, D. D. & MATSU'URA, J. 1985. A Bayesian approach to nonlinear inversion. *Journal of Geophysical Research*, **90**, 581–591.

KARATO, S.-I. & WU, P. 1993. Rheology of the upper mantle: a synthesis. *Science*, **260**, 771–778.

LAMBECK, K., JOHNSTON, P. & NAKADA, M. 1990. Holocene glacial rebound and sea-level change in NW Europe. *Geophysical Journal International*, **103**, 451–468.

——, ——, SMITHER, C. & NAKADA, M. 1996. Glacial rebound of the British Isles III: Constraints on mantle viscosity. *Geophysical Journal International*, **125**, 340–354.

MCCONNELL, R. K. 1968. Viscosity of the mantle from relaxation time spectra of isostatic adjustment. *Journal of Geophysical Research*, **73**, 7089–7105.

MITROVICA, J. X. 1996. Haskell [1935] revisited, *Journal of Geophysical Research*, **101**, 555–569.

—— & FORTE, A. M. 1997. Radial profile of mantle viscosity: results from the joint inversion of convection and postglacial rebound observables. *Geophysical Journal International*, **102**, 2751–2769.

—— & PELTIER, W. R. 1989. Pleistocene deglaciation and the global gravity field. *Journal of Geophysical Research*, **94**, 13 651–13 671.

—— & ——1991. On postglacial geoid subsidence over the equatorial oceans. *Journal of Geophysical Research*, **96**, 20 053–20 071.

—— & ——1995. Constraints on mantle viscosity based upon the inversion of post-glacial uplift data from the Hudson Bay region. *Geophysical Journal International*, **122**, 353–377.

OTA, Y., CHAPPELL, J., KELLEY, R., YONEKURA, N., MATSUMOTO, E., NISHIMURA, T. & HEAD, J. 1993. Holocene coral reef terraces and coseismic uplift at Huon Peninsula, Papua New Guinea. *Quaternary Research*, **40**, 177–188.

PARI, G. & PELTIER, W. R. 1995. The heat flow constraint on mantle tomography-based convection models: towards a geodynamically self-consistent inference of mantle viscosity. *Journal of Geophysical Research*, **100**, 12 731–12 751.

PELTIER, W. R. 1974. The impulse response of a Maxwell Earth. *Reviews of Geophysics and Space Physics*, **12**, 649–669.

——1976. Glacial isostatic adjustment II. The inverse problem. *Geophysicals Journal of the Royal Astronomical Society*, **46**, 669–706.

——1982. Dynamics of the ice-age Earth. *Advances in Geophysics*, **24**, 1–146.

——1983. Constraint on deep mantle viscosity from LAGEOS acceleration data. *Nature*, **304**, 434–436.

——1985. The LAGEOS constraint on deep mantle viscosity: results from a new normal mode method for the inversion of viscoelastic relaxation spectra. *Journal of Geophysical Research*, **90**, 9411–9421.

——1994. Ice-Age paleotopography. *Science*, **265**, 195–201.

——1995. Paleotopography of Ice-Age ice sheets. *Science*, **267**, 536–538.

——1996. Mantle viscosity and ice-age ice sheet topography. *Science*, **273**, 1359–1364.

——1997. Correction to the paper 'Glacial isostatic adjustment and earth rotation: refined constraints on the viscosity of the lower mantle', by W. R. Peltier and Xianhua Jiang, *Journal of Geophysical Research*, **102**, 10 101–10 103.

——1998*a*. Global sea level rise and glacial isostatic adjustment. *Global and Planetary Change*, in press.

——1998*b*. The inverse problem for mantle viscosity. *Inverse Problems*, in press.

——1998*c*. 'Implicit Ice' in the global viscoelastic and topographically self-consistent theory of glacial isostatic adjustment: implications for ice-age paleo-topography, *Geophysical Research Letters*, in press.

—— & ANDREWS, J. T. 1976. Glacial isostatic adjustment I. The forward problem. *Geophysical Journal of the Royal Astronomical Society*, **46**, 605–646.

—— & JIANG, X. 1996*a*. Glacial isostatic adjustment and earth rotation: refined constrains on the viscosity of the deepest mantle. *Journal of Geophysical Research*, **101**, 3269–3290.

—— & ——1996*b*. Mantle viscosity from the simultaneous inversion of multiple data sets pertaining to postglacial rebound. *Geophysical Research Letters*, **23**, 503–506.

—— & —— 1997. Mantle viscosity, glacial isostatic adjustment and the eustatic level of the sea. *Surveys in Geophysics*, **18**, 239–277.

——, FARRELL, W. E. & CLARK, J. A. 1978. Glacial isostasy and relative sea level: a global finite element model. *Tectonophysics*, **50**, 81–110.

——, FORTE, A. M., MITROVICA, J. X. & DZIEWONSKI, A. M. 1992. Earth's gravitational field: seismic tomography resolves the enigma of the Laurentian anomaly. *Geophysical Research Letters*, **19**, 1555–1558.

——, HILLAIRE-MARCEL, C. & PARI, G. 1998. Postglacial rebound at Richmond Gulf (Quebec), mantle viscosity, and the free air gravity anomaly over Hudson Bay, *Nature*, submitted.

PLATZMAN, G. W. 1971. Ocean tides and related waves. *In*: REID, W. A. (ed.) *Mathematical Problems in the Geophysical Sciences 2. Inverse Problems, Dynamo Theory and Tides*. Lectures in Applied Mathematics, American Mathematical Society, **14**, pp. 239–291,

SHACKLETON, N. J. 1967. Oxygen isotope analyses and Pleistocene temperatures re-addressed. *Nature*, **215**, 15–17.

——, BERGER, A. & PELTIER, W. R. 1990. *Transactions of the Royal Society of Edinburgh. Earth Sciences*, **81**, 251–261.

SIMONS, M. & HAGER, B. 1997. Localization of the gravity field and the signature of glacial rebound. *Nature*, **390**, 500–504.

STUIVER, M. & REIMER, R. J. 1993. Extended ^{14}C data base and revised Calib. 3.0 ^{14}C age calibration program. *Radiocarbon*, **35**, 215–230.

TARANTOLA, A. & VALETTE, B. 1982. Inverse problems = quest for information. *Journal of Geophysics*, **50**, 159–170.

—— & ——1984. Generalized non-linear inverse problems solved using the least squares criterion. *Reviews of Geophysics and Space Physics*, **20**, 219–232.

TARASOV, L. & PELTIER, W. R. 1997. Terminating the 100 kyr ice-age cycle. *Journal of Geophysical Research–Atmospheres*, **102**, D18, 21 665–21 693.

TUSHINGHAM, A. M. & PELTIER, W. R. 1991. ICE-3G: a new global model of late Pleistocene deglaciation based upon geophysical predictions of post-glacial relative sea level change. *Journal of Geophysical Research*, **96**, 4497–4523.

—— & ——1992. Validation of the ICE-3G model of Würm–Wisconsin deglaciation using a global data base of relative sea level histories. *Journal of Geophysical Research*, **97**, 3285–3304.

WU, P. & PELTIER, W. R. 1983. Glacial isostatic adjustment and the free air gravity anomaly as a constraint on deep mantle viscosity. *Geophysical Journal of the Royal Astronomical Society*, **74**, 377–449.

—— & ——1984. Pleistocene deglaciation and the Earth's rotation: a new analysis. *Geophysical Journal of the Royal Astronomical Society*, **76**, 202–242.

YODER, C. F., WILLIAMS, J. G., DICKEY, J. O., SCHUTZ, B. E., EANES, R. J. & TAPLEY, B. D. 1983. Secular variation of the Earth's gravitational harmonic J_2 coefficient from LAGEOS and non-tidal acceleration of Earth rotation. *Nature*, **303**, 757–762.